Title: Slow inactivation of sodium channel $Na_V1.2$ determines sleep quality

Authors: Yu Li[1*], Juhang Liu[1*], Kaiyue Yan[1*], Zhengbin Han[1], Chongchong Zhao[1], Laicai Zhang[1,2], Yanchen Liu[3], Mu Su[4], Bing Hu[1], Ying Li[1], Kaihang Ding[1], Yikui Zhao[1], Huiwen Tian[1], Qiang Sun[1], Guangfu Wang[1†], Jing Ma[1†] and Zhiqiang Wang[1†]

Affiliations:

[1]The HIT Center for Life Sciences, School of Life Science and Technology, Harbin Institute of Technology, Harbin, Heilongjiang, China.

[2]State Key Laboratory of Space Environment Interation with Matters, Space Environment Simulation Research Infrastructure, Harbin Institute of Technology, 150080, Harbin, China.

[3]Beijing Institute of Genomics, Chinese Academy of Sciences, Beijing 100101, China.

[4]School of Life Science and Technology, Harbin Institute of Technology, Harbin, Heilongjiang, China.

[*]These authors contributed equally to this work.

[†]Correspondence:

Guangfu Wang: wangguangfu@hit.edu.cn

Jing Ma: jingmawzq@foxmail.com

Zhiqiang Wang: zhiqiang.wangmj@foxmail.com

Abstract:

Sleep quantity and quality are homeostatically regulated through either cell-autonomous molecular mechanisms or neurocircuit-level processes[1-8]. The amount of non-rapid eye movement sleep (NREMS) is determined by a kinase signaling pathway operating at the transcriptional level within the posterior hypothalamus[9-11]. However, the core molecular mechanisms governing sleep quality in mammals remain elusive. Here, we identify the voltage-gated Na^+ channel $Na_v1.2$ as a critical modulator of NREMS slow-wave activity (SWA) —a macro-electrophysiological index of sleep need or quality[12-14]—across multiple sleep models. As a non-synaptic sleep-need-index-phosphoproteins (SNIPPs)[13], $Na_v1.2$—among the 12 Na^+ channel subunit proteins—undergoes unique cumulative phosphorylation at multiple sites upon time-course sleep deprivation (SD) or in *Sleepy* mice (two increased sleep need models)[9,13], and is dephosphorylated during subsequent sleep. These phosphosites cluster within a functional patch of the $Na_v1.2$ intracellular loop connecting transmembrane domains I and II—a region critical for dynamically regulating the channel's slow inactivation[15,16]. A single amino acid mutation in the S6 segment of $Na_v1.2$ domain III (N1467D) structurally impairs its slow inactivation, reduces baseline NREMS-SWA in wild-type mice, and markedly blunts AAV-*Camk2a-SLEEPY*-induced increases in NREMS-SWA. This mutation also attenuates SD -induced phosphorylation changes in the adult mouse brain proteome (including SNIPPs) and completely abolishes NREMS-SWA rebound following sleep loss. Mechanistically, $Na_v1.2$'s role in sleep regulation is physiologically dependent on the AKAP7α-RIIβ-PKA holoenzyme. Gabapentin—a clinically approved anticonvulsant[17]—promotes $Na_v1.2$ slow inactivation and increases NREMS-SWA in a $Na_v1.2$-dependent manner. Our results suggest that the AKAP7α-RIIβ-PKA-$Na_v1.2$ complex forms a compact homeostatic oscillator that senses global neuronal activity and specifically determine sleep quality (not sleep quantity),

highlighting a potential therapeutic target for developing mechanism-based sleep medicines.

MAIN TEXT

Elucidating the regulatory mechanisms underlying sleep is crucial for uncovering its intricate relationship with cognitive function and systemic physiological health[4,18-26]. Genetic studies in both fruit flies and mice have identified several sleep-regulatory protein kinases and phosphoprotein phosphatases (SRPKs and SRPPPs)—including protein kinase A (PKA)[27-29], casein kinase II (CK2)[30,31], extracellular signal-regulated kinase 1/2 (ERK1/2)[32,33], salt-inducible kinase 3 (SIK3)[9-11,34], calcium/calmodulin-dependent protein kinase II (CaMKII)[35-37], protein phosphatase 1 (PP1)[29], protein phosphatase 2A (PP2A)[22,38], and protein phosphatase 2B calcineurin (CaN)[29,39-42]—regulate sleep duration, timing, architecture, and homeostasis. Integrating advanced genetic, biochemical, electrophysiological, and quantitative electroencephalogram/electromyogram (EEG/EMG)-based sleep behavior analyses is necessary to identify the downstream effectors of these signaling pathways and their specific roles in sleep regulation[10,11,13,43].

NREMS-SWA, the EEG delta power band (1-4 Hz), is one of the most reliable markers for sleep need, depth, quality, and homeostasis[13,14]. It exhibits a quantitative and predictive relationship with prior wakefulness[10,12-14]; its proportional increase depends on both the duration and experience of prior wakefulness, and it decreases exponentially during the first several hours of sleep[12,13]. Quantitative trait loci analysis shows that the increase in NREMS-SWA is under strong genetic control[12]; however, the gene and the regulatory mechanism that fulfil these temporal changes and the proposed criteria[13,44] for the molecular substrate of sleep need remain unknown.

EEG/EMG-based forward-genetics analysis in randomly mutagenized mice identified a gain-of-function mutation in the *Sik3* gene that causes constitutively high NREMS-SWA and prolonged NREMS duration[9]. Together with other mouse genetic studies linking SRPKs (PKA[28,29,41], CaMKII[36,37]) and SRPPPs (PP2A[22,38], CaN[29,41,42]) to NREMS-SWA, these

findings highlight a potential phosphorylation-based feedback regulatory system (PBFRs) in sleep homeostasis[13,22]. While the direct substrates of these sleep-regulatory enzymes (which function as effectors in the sleep homeostatic system) remain unidentified, large-scale quantitative phosphoproteomic analyses have uncovered a set of phosphoproteins whose phosphorylation status is tightly linked to sleep–wake states[13,20,21,45,46]. Specifically, we identified 80 SNIPPs *via* cross-comparison of SD and *Sleepy* models, whose phosphorylation states parallel changes in sleep need[13]. Genetic perturbations of 12 SNIPPs induce sleep phenotypes in mice or humans, suggesting that SNIPPs include previously uncharacterized sleep regulators[13].

In this study, we identify the AKAP7α-RIIβ-PKA-$Na_v1.2$ complex as the central molecular machinery of the sleep homeostatic system. This complex meets the proposed criteria for the molecular substrates of sleep need; it undergoes cumulative phosphorylation at multiple sites and specifically enhances $Na_v1.2$ slow inactivation. We thus propose a regulatory mechanism that directly links molecular modifications to the channel's electrophysiological properties and changes in neuronal excitability—thereby mediating sleep homeostasis.

Use-dependent multisite phosphorylation of $Na_v1.2$

Genetic deficiencies in several SNIPPs are associated with sleep abnormalities—a common comorbidity of neurodevelopmental disorders[30,46]. However, the physiological functions of these SNIPPs and their underlying regulatory mechanisms in sleep remain unclear. Additionally, while 69 SNIPPs are annotated as synaptic proteins (highlighting a mechanistic link between synaptic homeostasis, synaptic transmission, and sleep–wake homeostasis[4,13,18]), we noted that two mouse Na^+ channels—$Na_v1.1$[47,48] and $Na_v1.2$[49,50] (encoded by *Scn1a* and *Scn2a*)—fall into the non-synaptic category **(Fig. 1a, Extended Data Fig. 1a)**. These channels are widely expressed in the central nervous system and regulate

action potential propagation and neuronal excitability, suggesting they may contribute directly to the control of NREMS-SWA—an established electrophysiological readout of sleep.

To examine the detailed correlation between phosphorylation changes of Na^+ channels and sleep need, we first performed quantitative phosphoproteomic analysis on brain samples from mice subjected to time-course sleep deprivation (tc-SD) at 1 h, 3 h, and 6 h **(Extended Data Fig. 1b, Supplementary Table 1a)**. Briefly, we calculated the slope and *P* value for 31,196 phosphopeptides in the tc-SD phosphoproteome **(Extended Data Fig. 1c)**, followed by overlap analysis with phosphopeptides from acute SD datasets—including comparisons of SD6/S6 (6 h of *ad libitum* sleep, ZT0–ZT6) and SD6/RS3 (3 h of recovery sleep following SD6) **(Extended Data Fig. 1d-f, Supplementary Table 1b-e)**.

This analysis revealed a unique and dominant phosphorylation pattern for $Na_v1.2$ **(Fig. 1b)**: among 49 overlapping phosphopeptides (from a total of 187 identified phosphopeptides) across 12 Na^+ channel family members, 6 phosphopeptides of $Na_v1.2$ (out of 29 total $Na_v1.2$ phosphopeptides) exhibited SD time-dependent increases in phosphorylation. These elevated phosphorylation levels were subsequently followed by dephosphorylation—either after 3 h of recovery sleep or when compared with the phosphorylation levels after 6 h of *ad libitum* sleep **(Fig. 1b, Extended Data Fig. 1e, f)**. Based on this sleep-associated dynamic phosphorylation profile, these phosphopeptides were designated as sleep-time-dependent class A phosphopeptides (STDPs-A, n=828) **(Fig. 1c, Extended Data Fig. 1e).**

To validate the functional link between $Na_v1.2$ STDPs-A and sleep need, we analyzed their phosphorylation status across multiple sleep models (**Fig. 1d**). Specifically, many STDPs-A sites were upregulated in models of increased sleep need (*Sleepy* mice and MK801-treated mice) and downregulated in models of decreased sleep need—including *Sleepy* and wild-type (WT) mice treated with the pan-SIK inhibitor

HG-9-91-0128 (HG)[13] (**Fig. 1d**). Thus, the temporal changes in $Na_v1.2$ STDPs-A phosphorylation closely correlate with sleep need across these distinct sleep models[13]. Given that $Na_v1.2$ is well established to regulate neuronal electrophysiology[49-52], its variable multisite phosphorylation may enable use-dependent regulation of channel gating and neuronal firing properties. This modulation of $Na_v1.2$ function, in turn, dynamically regulates integrated brain functions such as SWA—specifically by shaping cortical network synchronization and global slow oscillations[3,4,14] **(Fig. 1e)**.

Impaired slow inactivation of $Na_v1.2$ compromises NREMS-SWA

Most STDPs-A sites cluster within a functional domain of the $Na_v1.2$ DI–DII intracellular loop (**Fig. 1b, Supplementary Table 1e).** Previous heterologous cell-based studies have shown that this phosphorylation domain is critical for regulating $Na_v1.2$ slow inactivation[15,16]. Increased phosphorylation promotes the transition of $Na_v1.2$ into a slow inactivation state, and the asparagine residue at position 1467 (N1467) in the S6 segment of domain III (DIII) gates this process[15,16]. In heterologous cell expression systems, mutating N1467 to aspartic acid (N1467D) inhibits this state transition[15] **(Fig. 1e)**. To elucidate the role of $Na_v1.2$ slow inactivation in sleep regulation, we generated *Scn2a*^{N1467D} mutant mice using CRISPR/Cas9-mediated genome editing (**Extended Data Fig. 2a**). However, homozygous *Scn2a*^{N1467D} mutants exhibited neonatal lethality within 48 hours of birth **(Extended Data Fig. 2b)**, a phenotype consistent with that of *Scn2a-null* mice[53]. By contrast, heterozygous *Scn2a*$^{N1467D/+}$ mice (*N1467D/+*) were healthy and fertile, with normal body weight and $Na_v1.2$ protein abundance **(Extended Data Fig. 2c, d).** At baseline (BL), *N1467D/+* mice showed a significant reduction in NREMS-SWA despite normal total sleep amount **(Extended Data Fig. 2e-h)**; following SD, they also exhibited a trend toward reduced NREMS-SWA rebound **(Extended Data Fig. 2i-k)**.

To establish a *Scn2a*^{N1467D} homozygous model, we first generated an additional *Scn2a*$^{fl/fl}$

strain by inserting loxP sites downstream of exon 3 and upstream of exon 6 **(Extended Data Fig. 3a, b)**. We then crossed *Scn2a*$^{N1467D/+}$ and *Scn2a*$^{fl/fl}$ mice with CAGG$^{Cre\text{-}ERTM}$ transgenic mice, yielding two strains: *Scn2a*$^{N1467D/fl}$*; CAGG*$^{Cre\text{-}ERTM/+}$ (*N1467D*) **(Fig. 1f)** and *Scn2a*$^{fl/+}$*; CAGG*$^{Cre\text{-}ERTM/+}$ strain (*KO/+*) **(Extended Data Fig. 3c)**. Two weeks following tamoxifen (TAM) induction (initiated at 6 weeks of age), $Na_v1.2$ protein levels in both *TAM-N1467D* and *TAM-KO/+* mice were reduced to ~50% of those in WT mouse brain samples **(Fig. 1f-h, Extended Data Fig. 2c, 3d),** indicating that only the $Na_v1.2$ N1467D proteoform is present in *TAM-N1467D* mice.

NREMS-SWA is regulated in layer 5 pyramidal neurons of the cerebral cortex[10,11,14]. To assess how the $Na_v1.2$ N1467D mutation affects channel slow inactivation in *ex vivo* brain slices, we performed whole-cell patch-clamp recordings on layer 5 pyramidal neurons isolated from *TAM-N1467D* and WT mice[54,55] **(Extended Data Fig. 4c, d).** Compared to WT neurons, those from *TAM-N1467D* mice exhibited significant impairments in slow inactivation: across a range of voltages, sodium currents in *TAM-N1467D* neurons showed reduced slow inactivation, with delayed onset and accelerated recovery **(Fig. 1i-l).** Notably, *TAM-N1467D* mice displayed normal EEG/EMG activity and body weight **(Extended Data Fig. 4a, b)**, confirming that the *Scn2a*$^{N1467D/fl}$*; CAGG*$^{Cre\text{-}ERTM/+}$ strain is a valid genetic model for investigating the role of $Na_v1.2$ in sleep regulation.

Detailed analysis of sleep-wake behavior in *TAM-N1467D* mice revealed lower daily NREMS-SWA density **(Fig. 1m, n, Extended Data Fig. 4e),** indicative of reduced baseline sleep need. Furthermore, the elevation in NREMS-SWA induced by 6 hours of sleep deprivation (SD6) in WT mice was completely abolished in *TAM-N1467D* mice, but not in *TAM-KO/+* mice **(Fig. 1o, p and Extended Data Fig. 3i-k).** Importantly, *TAM-N1467D* mice showed normal wake and NREMS durations **(Extended Data Fig. 4f-i).** Together with observations from *N1467D/+* mice **(Fig. 1n, p)**, these results suggest that $Na_v1.2$ regulates

sleep need in an allele-dose-dependent manner.

To further confirm that $Na_v1.2$ functions in excitatory neurons to regulate NREMS-SWA, we performed adult-brain-chimeric (ABC) knockout of *Scn2a* by retro-orbital injection (ROI) of recombinant AAV-PHP.eB virus into adult *Scn2a*$^{N1467D/fl}$ mice[43,56] **(Fig. 2a)**. This virus drives systemic CRE recombinase expression under either the *Camk2a* or *mDlx* promoter to target excitatory neurons or inhibitory neurons, respectively[11,22]. Consistent with findings in *TAM-N1467D* mice, only *Camk2a-N1467D* mice exhibited reduced $Na_v1.2$ protein levels **(Fig. 2b, c)**, lower daily NREMS-SWA **(Fig. 2d, e and Extended Data Fig. 5a, f, g)**, and a blunted SD-induced NREMS-SWA rebound **(Fig. 2f, g and Extended Data Fig. 5l)**—with wake and NREMS durations remaining normal **(Extended Data Fig. 5b-e, h-k)**.

To test whether $Na_v1.2$ also acts downstream of the SLEEPY kinase, we expressed a constitutively active truncated SIK3 kinase (designated as sSLP) via ROI of AAV-PHP.eB virus carrying the *Camk2a-HA-sSLP* construct **(Fig. 2h)**. Immunoblotting confirmed sSLP expression and elevated phosphorylation of the AMP-activated protein kinase (AMPK) substrate motif[13,22] **(Fig. 2i).** Moreover, sSLP significantly enhanced $Na_v1.2$ slow inactivation—with changes in voltage dependence, onset, and recovery that were opposite to those observed in *TAM-N1467D* mice **(Fig. 2j-m).** As previously reported[9,13,22], forced expression of sSLP in WT mice altered sleep–wake behaviors: it shortened wake durations, increased NREMS, and elevated SWA during NREMS, REMS, and wakefulness **(Fig. 2n, o and Extended Data Fig. 6a-c).** Notably, all these sSLP-induced phenotypes were completely absent in *TAM-N1467D* mice **(Fig. 2p, q and Extended Data Fig. 6d-f)**—indicating that the sleep-regulatory gain-of-function of SLEEPY kinase acts through $Na_v1.2$.

$Na_v1.2$ functions as an effector in the sleep homeostatic system

A homeostatic system comprises three core elements: a sensor that periodically monitors the state variable, an integrator that analyzes this input to compute homeostatic drive, and an

effector responsible for acting on this drive to directly adjust the state variable[44]. From the perspective of sleep homeostatic signaling pathways: sleep regulatory substances (SRSs) —including adenosine, nitric oxide, hormones, prostaglandins, and cytokines—along with their corresponding receptors function as sensors[25,44,45,57-63]. SRPKs and SRPPPs act as integrators, processing sensory information and modifying downstream effectors[9-11,19,22,24,27-29,32-42,64]. Effectors—such as histone deacetylases, transcriptional regulators, and voltage-gated channels—dynamically regulate neuronal excitability *via* either transcriptional or electrophysiological mechanisms[9-11,21,27,35,43,65-68].

Quantitative EEG analyses suggest that $Na_v1.2$ serves as a modulator in the sleep homeostatic system, acting downstream of both behavioral and genetic manipulations **(Fig. 1 and 2)**. To further clarify the role of $Na_v1.2$ at the molecular level, we performed transcriptomic (bulk RNA sequencing), quantitative proteomic, and phosphoproteomic analyses using cerebral cortex samples from WT and *TAM-N1467D* mice under both S6 and SD6 conditions **(Extended Data Fig. 7a and Supplementary Table 2-4).** Relative to WT controls, *TAM-N1467D* samples showed a specific ~30–50% reduction in $Na_v1.2$ RNA levels, protein abundance, and the abundance of most $Na_v1.2$-derived peptides (**Fig. 3a-d, Extended Data Fig. 7b, c**)—that consistent with earlier immunoblotting results **(Fig. 1h)**.

For the *TAM-N1467D/*WT proteomic comparison, we quantified 187,613 unique peptides derived from 12,341 proteins; notably, very few proteins exhibited significant abundance changes under either S6 or SD6 conditions **(Fig. 3b, c, Extended Data Fig. 9a and b)**. In the phosphoproteomic analysis of *TAM-N1467D/*WT samples, we quantified 35,246 phosphopeptides from 5,062 phosphoproteins **(Fig. 3d and e, Extended Data Fig. 9c and d).** The $Na_v1.2$ N1467D mutation altered only a small fraction of the brain phosphoproteome, 3.2% under S6 conditions and 2.3% under SD6 conditions (**Fig. 3d and Extended Data Fig. 9c**).

To explore the potential molecular substrates or signaling pathways underlying NREMS-SWA changes in *TAM-N1467D* mice, we performed ΔPs analysis[13] to examine global phosphorylation state changes in proteins modulated by multisite cumulative phosphorylation[69], and kinase motif-enrichment (KME) analysis[22,70] to evaluate global changes in kinase signaling pathways. Through cross-comparison of multiple models with altered sleep need (SD, *Sleepy*, and pan-SIK inhibitor HG-treated *Sleepy*), SNIPPs[13] and sleep-related kinases (S-RKs)[22] (identified via KME analysis) are the molecular substrates or signaling pathways most functionally correlated with sleep need (**Extended Data Fig. 8a-j**). Notably, compared with the classic "increased sleep need" comparison (Slp/WT), both ΔPs analysis and KME analysis revealed minimal parallel changes in the ΔPs values of SNIPPs or enrichment of S-RKs in *TAM-N1467D* mice (**Fig. 3e-h, Extended Data Fig. 9d-g and Supplementary Table 4-5**). These results indicate that the attenuation of $Na_v1.2$ slow inactivation caused by the N1467D mutation is the direct factor responsible for the decreased basal sleep need—rather than effects mediated through other sleep regulatory pathways.

To evaluate differences in the homeostatic response between WT and *TAM-N1467D* mice, we analyzed their brain proteomes and phosphoproteomes under the SD6/S6 comparison. The brain proteomes of both WT (SD6/S6) and *TAM-N1467D* (SD6/S6) mice remained globally stable[42] (**Extended Data Fig. 9h-k)**. Consistent with previous findings[13], the brain phosphoproteome of WT mice showed significant changes in the SD6/S6 comparison (6.2%) **(Fig. 3i)**; however, SD-induced phosphoproteomic alterations were largely suppressed in *TAM-N1467D* samples (only 0.91%) **(Fig. 3j)**. Accordingly, the SD-induced cumulative phosphorylation of SNIPPs (**Fig. 3k, l**) and changes in S-RKs observed in WT mice were completely abolished in *TAM-N1467D* mice (**Fig. 3m-p**).

To further explore the potential mechanisms, we analyzed transcriptomic datasets from the *TAM-N1467D/*WT comparison. A total of 15,104 genes were quantified, but very few of

these genes exhibited significant changes in expression (only 0.35%) (**Fig. 3a, Extended Data Fig. 7b-e)**. Notably, several immediate early genes (IEGs)—including *Fos*, *Arc*, *Npas4* and *Egr2- Egr4*—were significantly downregulated in *TAM-N1467D* samples (**Fig. 3a, Extended Data Fig. 7e**). This significant and widespread downregulation of IEGs (a hallmark of reduced neuronal activity) suggests that neuronal activity is largely suppressed in *TAM-N1467D* mice, which might be the direct cause of the stable phosphoproteome and unaltered NREMS-SWA of *TAM-N1467D* after sleep lose.

Collectively, these EEG, electrophysiological, and molecular findings are logically consistent across different biological levels. The dramatic and specific changes in sleep quality in *TAM-N1467D* mice—reduced basal NREMS-SWA and the lack of SD-induced NREMS-SWA rebound—indicate that $Na_v1.2$, which functions as a downstream terminal effector in the sleep homeostatic system, is not only regulated by sleep but also gates other sleep-associated signaling pathways to control sleep homeostasis and related functions.

The PKA-RIIβ-$Na_v1.2$ pathway regulates sleep quality

Prediction of kinase-specific phosphorylation sites[70,71] identified 7 PKA substrate sites within the DI–DII loop of $Na_v1.2$ **(Fig. 4a and Supplementary Table 6a).** This finding was further validated *via* immunoblot analysis—utilizing an antibody targeting PKA-phosphorylated substrate motifs (pPKAsub)-performed after immunoprecipitation (IP) of endogenous $Na_v1.2$ protein under S6 and SD6 conditions (**Fig. 4b, c**). Moreover, co-IP assays revealed that $Na_v1.2$ interacts with the cAMP-dependent protein kinase catalytic subunit alpha (PKA-Cα), cAMP-dependent protein kinase type II-beta regulatory subunit (RIIβ), and membrane-anchored type II-specific A-kinase anchor protein 7 isoform alpha (AKAP7α)[16] **(Fig. 4d)**. We hypothesize that this AKAP7α-RIIβ-PKA-Cα-$Na_v1.2$ interaction mediates increased $Na_v1.2$ phosphorylation and enhanced slow inactivation *in vivo*[16,72] **(Fig. 4e)**.

To test this hypothesis, we administered a Stapled AKAP Disruptor Peptide (STAD-2)[73] *via* intracerebroventricular injection (i.c.v.) to specifically disrupt the interaction between RIIβ and AKAP7α in brain cells **(Fig. 4e)**. As expected, STAD-2 suppressed the interaction between RIIβ and $Na_v1.2$, altered the phosphorylation status of $Na_v1.2$ (**Fig. 4f**), and impaired $Na_v1.2$ slow inactivation—with changes in voltage dependence, onset, and recovery that were reminiscent of those observed in *TAM-N1467D* mice **(Fig. 4g-j).** Consistent with these molecular and electrophysiological alterations, STAD-2 treatment significantly reduced baseline NREMS-SWA and SD-induced NREMS-SWA rebound, while having no effect on NREMS duration (**Fig. 4k-n and Extended Data Fig. 10**). To further confirm the role of this complex, we expressed *Camk2a*-driven RIIβ or AKAP7α in WT mice **(Fig. 4o)**. Notably, only forced expression of RIIβ in WT mice increased NREMS-SWA, with no impact on NREMS duration **(Fig. 4p-r and Extended Data Fig. 11).** Thus, these results indicate that the AKAP7α-RIIβ-PKA holoenzyme—functioning as an integrator in the sleep homeostatic system—promotes $Na_v1.2$ phosphorylation and slow inactivation, and this process plays a critical role in regulating sleep quality.

Gabapentin improves sleep quality via $Na_v1.2$ in mammals

Clinically, over 80 distinct sleep disorders have been identified, with the most common including insomnia, narcolepsy, restless legs syndrome, and circadian rhythm disorders—all categorized in the *International Classification of Sleep Disorders* (ICSD). However, for most of these disorders, our understanding of their underlying mechanisms remains limited, and mechanism-based therapeutic options are even scarcer. A landmark example of mechanism-driven progress is the discovery of orexin/hypocretin and its role in narcolepsy: this finding advanced our understanding of the molecular and neurocircuitry mechanisms governing arousal regulation[60,61], and further led to the development of orexin antagonists, a novel class of clinically approved sedative-hypnotics for sleep-onset and sleep-maintenance

insomnia[25]. Building on this paradigm, our results demonstrate that the AKAP7α-RIIβ-PKA-$Na_v1.2$ pathway plays a central role in regulating sleep quality, and that $Na_v1.2$ slow inactivation is a critical node in this process—representing a potential therapeutic target for developing mechanism-based sleep medications.

Notably, $Na_v1.2$ is a validated target for numerous small-molecule modulators, which regulate its electrophysiological properties[17]. A previous study demonstrated that prolonged (3-day) treatment with gabapentin (GBP)—a clinically approved anticonvulsant—induces a hyperpolarizing shift in the inactivation of rat $Na_v1.2$ channels in a heterologous cell expression system[74]. Concurrently, a single i.p injection of GBP administered prior to light-phase onset increased NREMS-SWA and prolonged NREMS duration in adult rats[75]. Clinically, GBP is also used off-label to improve NREMS quantity in patients with primary insomnia[76], sensory nervous system disorders[77], and critically ill patients[78]. To validate the *in vivo* link between GBP, $Na_v1.2$, and sleep, we administered GBP *via* intraperitoneal injection (i.p.) to WT and *Camk2a-N1467D* mice **(Fig. 5a-m)**. In WT mice, GBP administration significantly increased NREMS-SWA (within the first 3 hours) and NREMS duration (within the first 4 hours) in a dose-dependent manner **(Fig. 5b–e, Extended Data Fig. 12a–d)**. Notably, unlike its effects in heterologous cell systems (which required prolonged treatment), GBP rapidly enhanced $Na_v1.2$ slow inactivation in *ex vivo* brain slices **(Fig. 5f–i),** which aligns with its rapid sleep-modulating effects in animals. Critically, the GBP-induced increase in NREMS-SWA was completely abolished in *Camk2a-N1467D* mice, whereas the GBP-induced increase in NREMS duration remained intact **(Fig. 5j–m, Extended Data Fig. 12e–k)**. Collectively, these results suggest that $Na_v1.2$ is the key target through which GBP regulates sleep quality (NREMS-SWA), whereas an alternative target protein may mediate its role in modulating sleep quantity (NREMS duration) in mammals.

Discussion

Sleep and wakefulness induce global phosphorylation changes in the brain proteome[13,20,46], and a subset of these alterations are tightly linked to the regulation of sleep homeostasis[13,18,20]. We previously hypothesized that the molecular substrates underlying sleep need must meet the following criteria: they should accumulate during wakefulness, dissipate with sleep, and track sleep pressure across different contexts; they should be globally regulated in the brain, and their manipulation should bidirectionally alter sleep need[13]. $Na_v1.2$ not only satisfies all these criteria but also functions in cortical excitatory neurons—consistent with recent cell-type-specific studies of sleep regulation[10,11,14]—further supporting its role as a critical terminal effector in the homeostatic system that controls sleep need **(Fig. 5n)**.

$Na_v1.2$ possesses three key molecular features that enable its function in regulating sleep homeostasis. First, multisite phosphorylation of $Na_v1.2$ provides sufficient capacity to monitor both the quantity and complexity of prior waking experiences through activity- or use-dependent phosphorylation. Concurrently, this post-translational modification enables graded regulation of the channel's electrophysiological properties[13,15,16,52]. Second, as a voltage-gated sodium channel, $Na_v1.2$ is pivotal for both the initiation and backpropagation of action potentials[15,16,49]. Specifically, cumulative phosphorylation of $Na_v1.2$ drives graded enhancement of its slow inactivation—a process that, in turn, suppresses neuronal firing[75,79]. This cascade directly links molecular-level modifications to functional changes in neuronal excitability. Third, PKA is one of the most critical kinases in signal transduction pathways that respond to diverse types of SRSs[27,29]. The plasma membrane-anchored protein complex composed of AKAP7α, PKA, RIIβ, and $Na_v1.2$ (AKAP7α-RIIβ-PKA-$Na_v1.2$)[16], forms a compact homeostatic oscillator. This specialized molecular machinery closely senses global neuronal activity and, in turn, modulates the balance between sleep and wake states. This

cell-autonomous phosphorylation-based feedback regulatory mechanism is likely vital for controlling neuronal excitability, cortical network synchronization, and global slow oscillations—operating both at the level of individual local neurons and across the entire brain[2-4,79]**(Fig. 5n)**. Through these feedback regulatory actions, the constituent proteins of PBFRs probably exert a protective function, safeguarding optimal synaptic homeostasis, cognitive performance, and even organismal survival[4,18,20,22,24,79].

The molecular mechanism governing circadian rhythms, primarily the transcriptional-translational negative feedback loops (TTFLs), have evolved to adapt to Earth's 24-hour rotation[26]. This rotational cycle regulates the timing of rest and activity for nearly all organisms on Earth, including the sleep-wake cycles of animals[26]. In animals, the nervous system senses the external environment and controls daily activities, consuming approximately 20% of the body's total energy (in the form of ATP)[80]. Most of this ATP is expended on maintaining neuronal firing to ensure proper signal transmission. Meanwhile, changes in the phosphorylation status of signaling transducers (e.g., synaptic SNIPPs) serve as the physical basis for fine-tuning information flow—both intracellularly and intercellularly—within neurons, and this process also consumes ATP. As the fundamental units of cognitive function, neurons depend on the restoration of their functional integrity during sleep to sustain subsequent waking periods via the PBFRs. Thus, the kinetic time scale of the phosphorylation-dephosphorylation cycle for these information transducers may have undergone convergent evolution across animals, allowing it to match the specialized functions of their respective nervous systems during sleep-wake cycles. A key function of sleep at the molecular level, therefore, is to maintain phosphoproteome homeostasis within the nervous system[22]—particularly in major neuronal cell types that are critical for long-range signal transmission and the control of daily activities[18,22].

Notably, PBFRs also operates in the animal circadian regulatory system. As core

components of the circadian oscillator, PERIOD proteins (PERs), undergo robust circadian fluctuations in multisite phosphorylation[81], a dynamic process modulated by the balance between CK1δ/ε and PP1[82]. This phosphorylation-dephosphorylation cycle, in turn, plays a central role in sustaining the TTFLs[81-83]. In addition, the KaiC phosphorylation cycle is an essential regulatory mechanism of the circadian clock in cyanobacteria[84], and the discovery of RUVBL2[85]—a P-loop NTPase that is the eukaryotic analog of KaiC—indicates that a similar molecular mechanism may exist in eukaryotes. Thus, the two-process model of sleep regulation—the major conceptual framework in sleep research proposed in 1982[1,5]—may converge on the same phosphorylation-based feedback regulatory mechanism. While the specific regulatory kinases, phosphatases, and molecular effectors may differ, and may also act in distinct brain regions and neuronal cell types, the core logic of the PBFRs is shared between sleep homeostasis and circadian rhythms. Intriguingly, several proteins function dually in both systems: for instance, SIK3 and HDAC4 participate in circadian regulation by modulating the timing of arousal at dark onset and circadian period through the SIK3–HDAC4 axis in the suprachiasmatic nucleus (SCN)[86]; in sleep regulation, they contribute to maintaining sleep homeostasis and the modulating NREMS amounts and depth[9-11]. Nav1.2 also modulates circadian rhythms and the spontaneous firing activity of SCN neurons[50]. Therefore, further investigating the roles of regulators and effectors in the PBFRs of these two processes—sleep drive (orchestrated by sleep homeostasis) and sleep-wake timing (governed by circadian rhythms)—will be critical for unraveling how the optimal timing, duration, and depth of sleep are coordinated[1,5] **(Fig. 5n)**.

The discovery of the orexin/hypocretin system and the subsequent development of its antagonists as a new generation of sedative-hypnotics have proven the transformative power of fundamental mechanism-driven sleep research[25,60,61,87]. Similarly, our findings demonstrate that the AKAP7α-RIIβ-PKA-$Na_v1.2$ pathway plays a key physiological role in regulating

sleep quality—acting via a specific mechanism that couples phosphorylation to the modulation of $Na_v1.2$ electrophysiological properties. This pathway therefore represents a promising therapeutic target for development of a new class of mechanism-based sleep medications, which could provide effective relief for various sleep disorders and their associated psychological comorbidities.

Acknowledgements

The authors thank Drs. Masashi Yanagisawa and Hiromasa Funato for providing the sleep analysis software; Drs. Bing Fu and Shuhui Ji from the National Center for Protein Sciences (Beijing), the core facilities of the HIT Center for Life Science, and the Laboratory of Space Life Science under the Space Environment Simulation and Research Infrastructure for their technical assistance.

This work was supported by grants from the National Major Project of China for Science and Technology Innovation 2030 – Brain Science and Brain-Inspired Technology (2021ZD0203400 to Z.W.); the National Natural Science Foundation of China (32071011 to Z.W., 31970912 to G.W.); the National Key R&D Program of China (2022YFA1604502 to Z.W. and G.W.); the Lingang Laboratory & National Key Laboratory of Human Factors Engineering Joint Grant (LG-TKN-202203-01 to Z.W.); the Frontiers Science Center for Matter Behavior in Space Environment (to Z.W.); the Fundamental Research Funds for the Central Universities (HIT.DZJJ.2023132 to J.L.); and the startup funds from the HIT Center for Life Science.

Author Contributions

Z.W. conceived the project. Yu L., J.L., and J.M. performed the sleep experiments. Yu L., J.L., and C.Z. conducted the mass spectrometric experiments. K.Y., Yu L., and G.W. carried out the electrophysiological experiments. Yu L., Z.H., L.Z., YC.L., M.S., B.H., Ying L., K.D., Y.Z., H.T. and Q.S. completed all other experiments. Yu L., J.L., J.M., and Z.W. analyzed the data and prepared the figures. Z.W. drafted the manuscript with contributions from all other authors.

Materials and Methods

Animals.

All animal experiments were conducted following procedures approved by the Harbin Institutional Animal Care and Use Committee of Harbin Institute of Technology (HIT/IACUC). The mice were housed under appropriate temperature and humidity conditions, with a 12-hour light-dark cycle. All mice were the C57BL/6J strain background, provided with adequate food and water, and housed until 8 to 12 weeks for experimentation. Point mutation mice $Scn2a^{N1467D}$ and, $Scn2a^{fl/fl}$ mice and $CAGG^{Cre\text{-}ERTM/+}$ mice were purchased from Cyagen Bioscience (Guangzhou, China). We crossed $CAGG^{Cre\text{-}ERTM/+}$ mice with $Scn2a^{N1467D/+}$ mice to obtain $Scn2a^{N1467D/+,\ Cre/+}$, and then crossed with $Scn2a^{fl/fl}$ mice to obtain $Scn2a^{N1467D/fl,\ Cre/+}$ mice.

STDPs analysis.

STDP analysis was performed using two datasets: (i) the time-course SD dataset (1 h, 3 h, 6 h of SD) and (ii) the acute SD dataset (SD6, RS3, and S6 conditions). For the time-course dataset, phosphopeptide abundances quantified in two independent TMT10-plex experiments were used to calculate the slope of abundance changes across SD time points **(Supplementary Fig. S1e)**. The significance of the slope was assessed by linear regression, yielding P values for each peptide. Phosphopeptides with $|\text{slope}| > 0.02$ and $P < 0.05$ were considered to exhibit significant time-dependent phosphorylation changes.

These candidates were then cross-analyzed with the acute SD dataset, in which phosphopeptide abundances were compared between SD6 and RS3 or between SD6 and S6 using statistical testing (Multiple t-test, $P < 0.05$). Phosphopeptides showing overlap between the two datasets were classified into five groups (A-E) according to their directional changes: slope^{+}RS3/S6^{-}, slope^{-}RS3/S6^{+}, slope^{+}RS3/S6^{+}, slope^{-}RS3/S6^{-}, and peptides without significant changes in either dataset **(Supplementary Fig. S1e)**.

Examples of each group are shown in **Fig. 1c**. For instance, $Na_v1.2$ S573/576 phosphopeptides exhibited SD time-dependent increases in phosphorylation that were reversed during RS3 and S6 (Group A). SPARCL1 S411 also showed SD-dependent increases, but phosphorylation continued to rise after RS3 and S6 (Group B). In contrast, ERMN S98 phosphorylation decreased with increasing SD duration and further declined after RS3 and S6, while FYCOL T372 also decreased during SD but increased after RS3 or S6. As an example of Group E, SBF1 S706 displayed no significant changes in phosphorylation levels cross conditions. A complete list of STDPs is provided in **Supplementary Table 1e**.

Genotyping.

Genomic DNA was prepared from toe biopsies (postnatal day 8–12) using a commercial rapid mouse genotyping kit (APE*BIO, K1025), which contains lysis buffer, balance buffer, proteinase K, and 2×Taq PCR Master Mix. Tissues were incubated in 60 µL lysis buffer with 0.6 µL proteinase K at 56 °C for 15 min and 95 °C for 30 min, cooled to 4 °C, and neutralized with 60 µL balance buffer. PCR was performed in 10 µL reactions using 0.5 µL lysate as template. For *N1467D/+* genotyping, amplicons were digested with MboI (recognition site GATC) in 20 µL reactions (10 µL PCR product, 3 µL buffer, 0.5 µL MboI, 6.5 µL water) at 37 °C for 60 min. PCR or digest products were resolved by agarose gel electrophoresis, and genotypes were assigned from the expected banding patterns.

Immunoprecipitation and immunoblotting.

Immunoprecipitation analysis was performed following the standard protocol with minor modifications[13]. Brain tissue was promptly excised from the mice, placed into cryopreservation tubes, and then stored in liquid nitrogen before being transferred to -80°C freezer. Both the glass homogenizers and the brain tissue lysis buffer were pre-cooled during the immunoprecipitation process. The lysis buffer consisted of 1% Triton X-100, 150 mM NaCl, 20 mM HEPES (pH 7.4), 2 mM $MgCl_2$, 1 mM EDTA, 15 mM NaF, 20 µM Leupeptin

hemisulfate, 10 μM Pepstatin A, 1 mM PMSF, 100 mM Sodium orthovanadate, 4 mM Sodium tartrate dibasic dihydrate, and a protease-phosphatase inhibitor cocktail. The brain tissue was placed in a glass homogenizer, 4 ml of lysis buffer was added, along with nuclease (#88702, Thermo). Homogenization was performed at 4°C. After lysis, the samples were incubated on ice for 30 minutes, after which the supernatant was collected and centrifuged at 13,000 g for 20 minutes at 4°C. The resulting supernatant was then subjected to BCA protein concentration assay. For immunoprecipitation, 35 mg of protein was mixed with 30 μl of Protein A/G PLUS-Agarose (sc-2003, Santa Cruz) and pre-incubated at 4°C for 30 minutes. The mixture was then centrifuged at 2,500 rpm for 5 minutes at 4°C, and the supernatant was collected. To the supernatant, 5 μl of anti-SCN2A ($Na_v1.2$) (#ASC-002, Alomone Labs) was added and incubated at 4°C for 1 h. Subsequently, 30 μl of Protein A/G PLUS-Agarose was added and incubated overnight at 4°C to isolate the immune complexes. Protein samples were separated and analyzed by SDS-polyacrylamide gel electrophoresis (PAGE) followed by Western blotting.

Immunoblotting was performed using the corresponding antibodies according to standard procedures. Antibodies utilized in this study encompassed anti-SCN2A($Na_v1.2$) (1:1000, #ASC-002, Alomone labs), anti-β-Tubulin (9F3) (1： 1000, #2128, Cell Signaling), anti-GAPDH (14C10) (1： 1000, #2118, Cell Signaling), guinea pig anti-SCN2A($Na_v1.2$) (1:1000,ASC-002-GP, ALomone labs), anti-phospho-AMPK Substrate Motif (LXRXX(S*/T*) (1:1000, #5759, Cell Signaling), anti-phospho-PKA Substrate (RRXS*/T*) (1:1000, #9624, Cell Signaling), PRKAR2B polyclonal antibody (1:1000, 28351-1-AP, Proteintech), DYKDDDDK Tag (D6W5B) Rabbit mAb (Binds to same epitope as Sigma-Aldrich Anti-FLAG M2 antibody) (1:1000, #14793, Cell Signaling), anti-Cre Recombinase (D7L7L)(1:1000, #15036, Cell Signaling), PKA C-α antibody(1:1000, #4782, Cell Signaling), anti-HA (C29F4) (1:1000, #3724, Cell Signaling) and anti-AKAP7 (1:1000, 12591-1-AP,

Proteintech).

EEG recording and sleep phenotype analysis.

The EEG recordings and sleep phenotype analysis were carried out as previously described[9,13,23]. All the mice that underwent EEG recording were male and at least 8 weeks old. During electrode implantation, the animals were anesthetized with continuous isoflurane and their heads were secured in a stereotaxic frame to maintain a horizontal position. The fur overlying the skull was shaved, and the skull surface was disinfected with hydrogen peroxide. Bregma (0, 0, 0) was marked as the origin with a marker pen. Four small holes were drilled in the skull at the following coordinates: (–1.27, 0), (–1.27, 5.03), (1.27, 5.03), and (1.27, 0). Stainless steel screw electrodes were placed at these sites and secured to the skull with dental cement (3M, USA). The scalp was then sutured. Following the surgical procedure, the mice were housed individually and allowed to recover for 7 days. After that, they were connected to recording cables and given an additional 7 days for habituation. The EEG/EMG recording started 14 days after the surgery and lasted for 4 consecutive days.

Sleep deprivation was performed starting at Zeitgeber Time 0 (ZT0). Mice were kept awake by gentle handling, including lightly tapping the cage, touching the animals with a brush, or introducing novel objects as needed. This procedure was maintained until ZT6 to effectively prevent sleep without causing undue stress. The EEG/EMG data were first analyzed semi-automatically and then manually corrected to ensure accuracy. The Fast Fourier transform was applied to the EEG data within the frequency range of 1 to 30 Hz and in 20-second epochs. The waking state was defined as featuring low-amplitude, fast EEG coupled with high-amplitude, variable EMG. NREMS was characterized by high-amplitude, delta (1-4 Hz) frequency EEG accompanied by low muscle tone. REMS was characterized by dominant theta (6-9 Hz) frequency EEG along with muscle atonia. Absolute and relative power spectrum analyses were performed for each ZT period. The relative power spectrum

(%) was calculated by expressing the EEG power in each frequency band as a percentage of the total power across all frequency bands (1-30 Hz). The duration and power density of NREMS, REMS, and the waking state were averaged on an hourly basis from ZT0 to ZT23. All data analyses were performed with the experimenters blinded to genotype. Animals with unreadable EEG signals were excluded from the study to ensure data quality.

Tamoxifen and gabapentin supplementation.

Tamoxifen (#S1238, Selleck) was dissolved in corn oil to prepare a solution with a concentration of 20 mg/ml. When the mice reached 6 weeks, tamoxifen was intraperitoneally administered at a dose of 75 mg/kg to *Scn2a*$^{N1467D/fl}$, $^{Cre/+}$ mice and their littermate *Scn2a*$^{fl/+}$ mice for five consecutive days. Tamoxifen treatment did not affect body weight in either genotype.

Gabapentin (#PHR1049, Sigma) was dissolved in 0.9% saline at final concentrations of 3 mg/mL and 12 mg/mL and administered intraperitoneally at ZT23.5, corresponding to doses of 30 mg/kg and 120 mg/kg.

Brain slice preparation and electrophysiology.

The preparation of motor cortical slices for electrophysiological recordings followed protocols established in previous studies[54,55]. Whole-cell patch-clamp recordings were conducted at 32-34°C using Model 2400 amplifiers (A-M Systems). The data were analyzed using Igor Pro 6 (WaveMetrics). All brain slices were obtained from 8-week-old-mice. After decapitation, brain tissue was quickly extracted and immersed in ice-cold (0–4°C) artificial cerebrospinal fluid (ACSF) solution. The ACSF (pH 7.4) contained 119 mM NaCl, 2.5 mM KCl, 1 mM NaH_2PO_4, 26 mM $NaHCO_3$, 1 mM $MgCl_2$, 25 mM glucose, and 2 mM $CaCl_2$, with an osmolarity of 300-305 mOsm and saturated with 95% O_2 and 5% CO_2. During recordings of slow inactivation in brain slices from WT mice intraperitoneally injected with gabapentin (120 mg/kg), 300 μM gabapentin was also added to the ACSF. The brain tissue

was then subsequently mounted on a custom-made slicing platform with a 10° bevel and sliced into 400 μM coronal sections using a VT1200S vibratome (Leica Biosystems). Following this, the slices were incubated in oxygenated ACSF at 37.0°C ± 0.5°C for 20 minutes, and then incubated at room temperature until being transferred to the recording chamber.

In this experiment, all recordings were from layer 5 pyramidal neurons in the motor cortex. Electrodes were pulled from borosilicate glass using a P-97 puller (Sutter Instruments), with resistances ranging from 4–7 MΩ. The intracellular solution contained 10 mM HEPES, 2.5 mM $MgCl_2$, 20 mM CsCl, 115 mM $CsMeSO_3$, 4 mM Na_2-ATP, 0.4 mM Na-GTP, 10 mM Na-Phosphocreatine, 0.6 mM EGTA and 0.1 mM Spermine (pH 7.25), with an osmolarity of 300 mOsm/kg. A motorized micromanipulator (Junior Multpatch, Lugis & Neumann) was used to guide the electrodes to the target cells for data acquisition. Electrophysiological data acquisition and stimulation commands were managed through synchronized LIH 8+8 data acquisition interface boards (HEKA Instruments), with operation controlled by Igor Pro 6[55].

To study the voltage dependence of slow inactivation, a prepulse was applied for 5 s, stepping from a holding potential of -100 mV to the indicated potentials ranging from -120 mV to 20 mV. Following this, the cells were repolarized to -100 mV for 20 ms to allow recovery from fast inactivation. A second test pulse to 10 mV was then applied for 10 ms, and evoked currents were recorded. To study the onset of slow inactivation, the above protocol was modified so that the prepulse had a fixed voltage (10 mV) but with different durations (ranging from 10 ms to $10^{3.8}$ ms, following an exponential increase pattern). To study the recovery from slow inactivation, both the voltage and the duration of the prepulse were fixed (10 mV, 5 s), but the time interval between the prepulse and the test pulse varied.

Plasmids construction and AAV packaging.

Mouse open reading frame (ORF) of sSLP (Sik3, A260-K527, NM_027498) was produced

579 from Comate Bioscience. Human AKAP7α and pAAV-Camk2a-PRKAR2B-3×FLAG was
580 purchased from Miaoling Biology (P4655, P80292, respectively). The
581 pAAV-Camk2a-AKAP7α-3×FLAG was generated by replacing PRKAR2B in
582 pAAV-Camk2a-PRKAR2B-3×FLAG with AKAP7α. The Cre recombinase and mDlx
583 promoter were from pAAV-U6-sgRNA-pCBh-Cre-WPRE-hGHpA (60229, Addgene) and
584 pAAV-mDlx-GFP-Fishell-1 (Addgene, 83900). The pAAV-Camk2a-Cre and pAAV-mDlx-Cre
585 were constructed using restriction enzyme digestion and ligation.
586 Based on previous methods[22,43,56] for AAV packaging and purification, with some
587 improvements made, pAAV-PHP.eB, pAAV-helper, and the pAAV vector containing the
588 target gene sequence were co-transfected into AAVpro 293T cells using polyethyleneimine
589 "Max" (PEI MAX) transfection reagent. Twelve hours after the transfection, the original
590 culture medium was replaced with serum-free DMEM. After incubating for 5 days, the
591 supernatant was collected and the cells were harvested with a cell scraper. The mixture was
592 then transferred to a 50 ml centrifuge tube and centrifuged at 13,000 rpm for 10 minutes at
593 room temperature. Subsequently, the supernatant was transferred to a new 50 mL centrifuge
594 tube. Meanwhile, the remaining cell pellet was resuspended in 1 ml of phosphate buffered
595 saline (PBS), subjected to 5 freeze-thaw cycles, and then centrifuged at 13,000 rpm for 20
596 minutes to obtain the supernatant. The supernatants from both centrifugations were filtered
597 through a 0.45 μm filter into a 50 mL centrifuge tube. Next, 6 ml of sterile 14% bovine serum
598 albumin (BSA) were added to reach a final concentration of 3%. Then, 7 ml of pre-chilled
599 PEG8000 solution (4X) were added, mixed thoroughly, and left at 4°C overnight (not
600 exceeding 24 hours). On the following day, the 50 ml centrifuge tube was centrifuged at
601 3,500 g for 1 hour at 4°C. After that, the supernatant was discarded, and the pellet was
602 centrifuged again at 3,500 g for 1 minute at 4°C. The pellet was then resuspended in 1.5 ml
603 PBS by gentle pipetting. The concentrated virus solution was frozen at -80°C for future use.

The virus titers were determined using linearized genomic plasmids as standards. For the injection of AAV virus into mice, the mice were first deeply anesthetized with isoflurane and then injected with 100 µl of AAV virus solution (1.0×10^{12} vg/ml) through the retro-orbital sinus.

Transcriptomic analysis.

For RNA-seq analysis, the mouse cerebral cortex and hippocampus were rapidly dissected at the same time point ten days after Tamoxifen induction, immediately flash-frozen in liquid nitrogen, and subsequently submitted to Novogene for sequencing. Total RNA was extracted from samples using TRIpure Isolation Reagent (94015120, Roche, Mannheim, Germany). For each sample, 1 µg of RNA was used for library preparation. Sequencing libraries were generated using the NEBNext® Ultra™ RNA Library Prep Kit for Illumina® (NEB, USA) according to the manufacturer's instructions, and index codes were added to each sample. Clustering of the index-coded libraries was performed on a cBot Cluster Generation System using the TruSeq PE Cluster Kit v3-cBot-HS (Illumina) according to the manufacturer's protocol. After cluster generation, the libraries were sequenced on an Illumina HiSeq X Ten platform to generate 150 bp paired-end reads. High-quality paired-end reads were aligned to the mouse reference genome (GRCm38, Ensembl release 90) using Hisat2 (v2.0.4), and gene expression levels were quantified with HTSeq (v0.9.1).

All raw sequencing data were subjected to quality assessment using FastQC, and the results indicated high overall quality. Gene expression analysis was performed with edgeR. Lowly expressed genes were filtered based on CPM, requiring each gene to have at least 20 counts in at least 40% of the samples **(Extended Data Fig. 7b).** Normalization was conducted using the trimmed mean of M-values (TMM) method to correct for biases caused by differences in sequencing depth or sample composition. Dispersion estimates were obtained, and expression levels for each gene were modeled using a generalized linear model. Differential expression

between groups was assessed with likelihood ratio tests. Differentially expressed genes (DEGs) were defined as those with FDR < 0.05 and $|\log_2 FC| > 1$ **(Supplementary Table 2b)**.

Tissue collection and sample preparation for mass spectrometry.

The preparation of mass spectrometry samples was conducted according to previously described procedures with certain modifications[13]. Wild type mice and *N1467D* mice were subjected to two conditions: normal sleep for 6 h (S6) and sleep deprivation for 6 h (SD6). The mice brains were rapidly extracted, placed into cryovials, and immediately frozen in liquid nitrogen. Subsequently, they were transferred to a -80°C freezer for long-term storage. The brain tissue was lysed using a buffer consisting of 50 mM HEPES (pH 8.5), 150 mM NaCl, 2 mM $MgCl_2$, and 1% SDS. A pre-chilled glass homogenizer was used to grind the brain tissue; initially, 5 mL of the brain tissue lysis buffer and nuclease (Thermo) were added, followed by 2 mL of 10% SDS buffer. After homogenization, the samples were incubated for 30 minutes followed by centrifugation at 13,000 g for 20 minutes at room temperature. The supernatant was transferred to a new 15 mL tube. Total protein concentration was determined using the BCA™ Protein Assay (Pierce). Dithiothreitol was added to the protein lysate for reduction, followed by alkylation with iodoacetamide. The samples were then processed using the chloroform-methanol precipitation method and subsequently resuspended in 8 M urea buffer. Following this, the samples were digested with recombinant Lys-C for 2 hours, diluted with 100 mM NH_4HCO_3 buffer (pH 7.8) to a final concentration of 2 M urea, and further digested with trypsin (Promega) at room temperature for 12 hours. The digestion was terminated with 1% trifluoroacetic acid (TFA). The resulting peptides were desalted using C18 solid-phase extraction and then concentrated to near dryness by vacuum centrifugation.

The desalted peptides were resuspended in 1.2 mL of phosphopeptide binding buffer [2 M lactic acid/50% acetonitrile (ACN)], and centrifuged at 13,000 g for 20 minutes. The supernatant was transferred to a new tube. TiO_2 beads were first washed three times with the

phosphopeptide binding buffer, then added to the supernatant and incubated at room temperature for 1 hour. The mixture was then washed twice with 2 M lactic acid/50% ACN, followed by two washes with 50% ACN/0.1% TFA. Elution was performed twice with 500 µL of elution buffer (50 mM K_2HPO4, pH 10), followed by acidification with 20% TFA, desalting, and concentration to dryness by vacuum centrifugation.

The enriched phosphopeptides were resuspended in 200 mM HEPES (pH 8.5) buffer. The concentration of phosphopeptides was determined using the BCA assay. Approximately 50 µg of each sample was labeled with Tandem Mass Tags (TMT) at room temperature for 1 hour. Labeling was quenched with 5% hydroxylamine, and the TMT-labeled samples were pooled into a single tube, acidified with 20% TFA, desalted, and concentrated to near dryness by vacuum centrifugation. The samples were then subjected to HPLC fractionation using a 400 µL buffer A (1% ACN, 10 mM ammonium formate, pH 9.5) and an Agilent 300 Extend C18 column (5 µM particles, 4.6 mM inner diameter, 150 mm length). After HPLC fractionation, the samples were acidified with 20% TFA and concentrated to dryness by vacuum centrifugation. The resulting samples were desalted using Stage Tips, concentrated to dryness, and resuspended for LC/MS analysis.

Mass spectrometry data acquisition and processing.

For liquid chromatography tandem mass spectrometry (LC-MS/MS) analysis, TMT-labeled peptides were separated using a 120-minute gradient elution at a flow rate of 0.300 mL/min through an Ultimate 3000 system, which was connected directly to a Thermo Orbitrap exploris 480 mass spectrometer. The analytical column was a fused silica capillary (75 µm ID, 150 mm long; Upchurch, Oak Harbor, WA) packed with C-18 resin (300 Å, 5 µm; Varian, Lexington, MA). Mobile phase A consisted of 0.1% formic acid, and mobile phase B consisted of 100% acetonitrile and 0.1% formic acid. The Orbitrap exploris 480 mass spectrometer was operated in data-dependent acquisition mode using Xcalibur 4.5 software.

The Orbitrap performed a single full-scan mass spectrometry analysis (300-1800 m/z, 60,000 resolution), followed by a 2 s of data-dependent MS/MS scans in an ion-guided multipole with a standard collision energy of 36%.

Mass spectra obtained from each LC-MS/MS analysis were compared with the mouse database using the Sequest HT algorithm in Proteome Discoverer software (PD, version 2.5). The search criteria were as follows: full tryptic trypsin specificity was required; one missed cleavage was allowed; oxidation (M) was set to variable modification; carbamidomethylation (C) and TMT-6 plex (K- and N-terminal) were set to fixed modification; and the precursor ion mass tolerance was set to 20 ppm for all MS data and 0.02 Da for all MS/MS spectra. Peptide False Discovery Rate (FDR) was calculated using Percolator provided with PD 2.5. Peptide spectra were considered correctly matched when the q value was less than 1%. Relative protein quantification was performed by PD software based on the intensity of TMT reporter ions. Quantification was performed only for proteins with two or more unique peptide matches. Peptides assigned to only a single proteome were considered unique. Protein ratios were calculated based on the median number of all peptides belonging to the protein. The precision of quantification is expressed by the variability of the protein ratios.

Mass spectrometry data analysis.

Protein isoforms were considered distinct proteins in proteomic analysis. Phosphopeptides were utilized in phosphoproteomic analysis, which includes unique forms and composite forms (containing two or more phosphorylation sites). Standardized abundance data obtained from experiments are combined (summed) to generate unique protein or phosphopeptide IDs along with the aggregated abundance values, which are then scaled to ensure that the average abundance for each sample is one. Standardized data from different experiments were integrated based on a unique sample ID for comparative purposes (e.g., SD6/S6 WT). Subsequently, the "$\log_2$(fold change)" values were generated using the means of each

experimental group; statistical significance was analyzed through multiple unpaired t-tests (*P* values). A statistical significance threshold of $P < 0.01$ was applied in the proteomic analysis, whereas for the phosphoproteomic analysis of N1467D mice, where overall changes were relatively limited, the threshold was slightly relaxed to $P < 0.02$ to facilitate downstream investigations. Detailed descriptions and datasets of all proteomic experiments are listed in **Supplementary Table 3**, while datasets from all phosphoproteomic experiments are listed in **Supplementary Table 4**.

The calculation method for the change in phosphorylation state (ΔPs) value is as previously described[13], which is equal to the sum of the "$\log_2$(fold change)" values of all phosphorylated peptides that show statistically significant changes ($P < 0.02$). These phosphorylated peptides come from all protein isoforms encoded by the same gene. If none of the *P* values for the phosphorylated peptides are less than 0.02, then the ΔPs value is zero. A complete description of the ΔPs analysis and the dataset are listed in Table S6.

Kinase motif enrichment analysis.

Kinase enrichment analysis was performed using the Python package kinase-library (https://kinase-library.phosphosite.org). In brief, phosphopeptides were converted into single-site patterns, with each site in multi-phosphorylated peptides assigned the same log2FC and statistical values. Sequence windows of 15 amino acids (7 residues upstream and downstream of the site) were generated, with "-" used as a placeholder when the sequence was shorter. These sequence windows, along with their corresponding log2FC and *P* values, were analyzed using kinase-library with parameters lfc_thresh = 0.3 and lfc_thresh = 0.02, while all other parameters were kept at default. Enrichment analyses were performed separately for Ser/Thr and Tyr kinases, and the results were subsequently combined for downstream analysis. Complete kinase enrichment results are provided in **Supplementary Table 5b**. Sleep-related kinases (S-RKs) were defined as those showing significant changes

in Slp/WT and also in SD6/RS3 or SD6/S6 comparisons. Kinases that were consistently enriched were designated as S-RKs-E, while those consistently depleted were designated as S-RKs-D **(Supplementary Fig. S7i and Supplementary Table 5c)**. Changes in S-RKs across different comparisons were assessed, and the proportion of concordantly changed S-RKs was used for Chi-square testing **(Fig. 3i)**. S-RKs exhibiting significant changes across multiple comparison groups were further analyzed by linear regression to test the correlation of kinase changes, with slopes, R^2, and *P* values reported.

S-RKs and kinase motif–enrichment correlation analysis help to elucidate the kinase change patterns across different sleep models: comparisons with elevated sleep need, such as Slp/WT and SD6/RS3, exhibited a higher proportion of concordant S-RK changes and showed a significant positive correlation ($P < 0.01$); in contrast, in the HG/Veh-Slp model with reduced sleep need, concordant S-RKs were markedly decreased compared to Slp/WT, along with a significant negative correlation. This indicates that S-RKs play an important role in sleep need changes induced by Slp, SD6, and HG. Conversely, in the N1467D model, although SWA was reduced and the proportion of concordant S-RKs was significantly decreased, no correlation with kinase changes in Slp/WT was observed. This provides important insights into the molecular alterations in the brains of N1467D mice.

PKA substrate site prediction.

PKA substrate site prediction for $Na_v1.2$ was performed using both the kinase-library package and the Group-based Prediction System (GPS). For kl-library, $Na_v1.2$ sites underwent the same preprocessing as described above, with a percentile threshold set at 95. The full-length mouse $Na_v1.2$ protein sequence was also analyzed using GPS, with a cutoff of 22.9 as recommended by the software. The predicted PKA scores for the detected phosphorylation sites in the phosphoproteomic analysis are presented in **Supplementary Table 6a**.

Cannula implantation and injection.

In the experiment involving intracerebroventricular injection via cannulation, all the mice were male and were at least 8 weeks old. The mice were kept under continuous anesthesia with isoflurane, and their heads were fixed in a stereotaxic frame to ensure accurate positioning. With the Bregma point (0, 0, 0) set as the coordinate origin, burr holes were drilled at specific cranial locations using a handheld drill. A cranial cannula was implanted at coordinates (2, –0.5, –1.45) with a 30° insertion angle. Electrodes were implanted at cranial coordinates (–1.27, 0, 0), (–1.27, 5.03, 0), (1.27, 5.03, 0), and (1.27, 0, 0).

Statistical methods.

All experiments were carried out with biological replicates, and each experiment was independently conducted at least twice to ensure the reliability. Mice were randomly assigned numbers and blindly grouped for EEG/EMG, as well as subsequent data processing. All data are presented as mean ± s.e.m. The number of animals or samples used in each experiment is reported in the figure legends. The intensity of protein bands was quantified using Image J (NIH) software. Statistical analysis was performed using GraphPad Prism and Microsoft Excel. Two-way analysis of variance (ANOVA) was employed, followed by Sidak's test for comparing multiple means, Fisher's LSD test for pairwise mean comparisons when ANOVA shows significant differences between groups. Unpaired two-tailed t-tests were used for comparisons between two independent groups, while paired two-tailed t-tests were applied for within-subject comparisons. For multiple group comparisons, ordinary one-way ANOVA with Fisher’s LSD post hoc test was used, and repeated-measures one-way ANOVA with Fisher’s LSD was applied when appropriate. For experiments involving two independent variables, two-way ANOVA was performed, followed by Sidak’s, Dunnett’s, or Fisher’s LSD post hoc tests, as specified. Fisher’s LSD was applied only when the omnibus ANOVA indicated a significant difference. The complete sample size, statistical analysis methods, and results for each comparison are reported in the figure legends and **Supplementary Table 7**.

Reference

1 Borbely, A. A. A two process model of sleep regulation. *Human neurobiology* **1**, 195-204 (1982).

2 Vyazovskiy, V. V. *et al.* Local sleep in awake rats. *Nature* **472**, 443-447 (2011).

3 Vyazovskiy, V. V. & Harris, K. D. Sleep and the single neuron: the role of global slow oscillations in individual cell rest. *Nat Rev Neurosci* **14**, 443-451 (2013).

4 Tononi, G. & Cirelli, C. Sleep and the price of plasticity: from synaptic and cellular homeostasis to memory consolidation and integration. *Neuron* **81**, 12-34 (2014).

5 Borbely, A. A., Daan, S., Wirz-Justice, A. & Deboer, T. The two-process model of sleep regulation: a reappraisal. *J. Sleep Res.* **25**, 131-143 (2016).

6 Adamantidis, A. R. & de Lecea, L. Sleep and the hypothalamus. *Science* **382**, 405-412 (2023).

7 Ma, C. & Dan, Y. The how and why of sleep: Motor theory and catecholamine hypothesis. *Neuron* (2025).

8 Liu, K. *et al.* Lhx6-positive GABA-releasing neurons of the zona incerta promote sleep. *Nature* **548**, 582-587 (2017).

9 Funato, H. *et al.* Forward-genetics analysis of sleep in randomly mutagenized mice. *Nature* **539**, 378-383 (2016).

10 Kim, S. J. *et al.* Kinase signalling in excitatory neurons regulates sleep quantity and depth. *Nature* **612**, 512-518 (2022).

11 Zhou, R. *et al.* A signalling pathway for transcriptional regulation of sleep amount in mice. *Nature* **612**, 519-527 (2022).

12 Franken, P., Chollet, D. & Tafti, M. The homeostatic regulation of sleep need is under genetic control. *J. Neurosci.* **21**, 2610-2621 (2001).

13 Wang, Z. *et al.* Quantitative phosphoproteomic analysis of the molecular substrates of sleep need. *Nature* **558**, 435-439 (2018).

14 Krone, L. B. *et al.* A role for the cortex in sleep-wake regulation. *Nat Neurosci* **24**, 1210-1215 (2021).

15 Chen, Y. A., Yu, F. H., Surmeier, D. J., Scheuer, T. & Catterall, W. A. Neuromodulation of Na+ channel slow inactivation via cAMP-dependent protein kinase and protein kinase C. *Neuron* **49**, 409-420 (2006).

16 Cantrell, A. R. *et al.* Molecular mechanism of convergent regulation of brain Na(+) channels by protein kinase C and protein kinase A anchored to AKAP-15. *Mol Cell Neurosci* **21**, 63-80 (2002).

17 Müller, P., Draguhn, A. & Egorov, A. V. Persistent sodium currents in neurons: potential mechanisms and pharmacological blockers. *Pflug Arch Eur J Phy* **476**, 1445-1473 (2024).

18 Cirelli, C. & Tononi, G. Linking the need to sleep with synaptic function. *Science* **366**, 189-190 (2019).

19 Ode, K. L. & Ueda, H. R. Phosphorylation Hypothesis of Sleep. *Frontiers in psychology* **11**, 575328 (2020).

20 Bruning, F. *et al.* Sleep-wake cycles drive daily dynamics of synaptic phosphorylation. *Science* **366** (2019).

21 Diering, G. H. *et al.* Homer1a drives homeostatic scaling-down of excitatory synapses

during sleep. *Science* **355**, 511-515 (2017).

22 Ma, J. *et al.* Sleep prevents brain phosphoproteome disruption to safeguard survival. *Cell Discov* **11** (2025).

23 Lou, T. *et al.* Hyper-Activation of mPFC Underlies Specific Traumatic Stress-Induced Sleep-Wake EEG Disturbances. *Frontiers in neuroscience* **14**, 883 (2020).

24 Sang, D. *et al.* Prolonged sleep deprivation induces a cytokine-storm-like syndrome in mammals. *Cell* **186**, 5500-5516.e5521 (2023).

25 Muehlan, C., Roch, C., Vaillant, C. & Dingemanse, J. The orexin story and orexin receptor antagonists for the treatment of insomnia. *Journal of Sleep Research* **32** (2023).

26 Rasmussen, E. S., Takahashi, J. S. & Green, C. B. Time to target the circadian clock for drug discovery. *Trends in biochemical sciences* **47**, 745-758 (2022).

27 Hendricks, J. C. *et al.* A non-circadian role for cAMP signaling and CREB activity in Drosophila rest homeostasis. *Nat Neurosci* **4**, 1108-1115 (2001).

28 Hellman, K., Hernandez, P., Park, A. & Abel, T. Genetic evidence for a role for protein kinase A in the maintenance of sleep and thalamocortical oscillations. *Sleep* **33**, 19-28 (2010).

29 Wang, Y. M. *et al.* Postsynaptic competition between calcineurin and PKA regulates mammalian sleep-wake cycles. *Nature* **636**, 412-+ (2024).

30 Lin, J. M. *et al.* A role for casein kinase 2α in the circadian clock. *Nature* **420**, 816-820 (2002).

31 Maier, B. *et al.* A large-scale functional RNAi screen reveals a role for CK2 in the mammalian circadian clock. *Gene Dev* **23**, 708-718 (2009).

32 Vanderheyden, W. M., Gerstner, J. R., Tanenhaus, A., Yin, J. C. & Shaw, P. J. ERK phosphorylation regulates sleep and plasticity in Drosophila. *PLoS One* **8**, e81554 (2013).

33 Mikhail, C., Vaucher, A., Jimenez, S. & Tafti, M. ERK signaling pathway regulates sleep duration through activity-induced gene expression during wakefulness. *Science signaling* **10** (2017).

34 Li, Y. *et al.* Sleep need, the key regulator of sleep homeostasis, is indicated and controlled by phosphorylation of threonine 221 in salt-inducible kinase 3. *Genetics* **225** (2023).

35 Tatsuki, F. *et al.* Involvement of Ca(2+)-Dependent Hyperpolarization in Sleep Duration in Mammals. *Neuron* **90**, 70-85 (2016).

36 Kon, K. *et al.* Cortical parvalbumin neurons are responsible for homeostatic sleep rebound through CaMKII activation. *Nature communications* **15** (2024).

37 Tone, D. *et al.* Distinct phosphorylation states of mammalian CaMKIIβ control the induction and maintenance of sleep. *Plos Biology* **20** (2022).

38 Zhou, S. *et al.* PP2Acα regulates sleep amount and sleep homeostasis in mice. *Commun Biol* **8** (2025).

39 Nakai, Y. *et al.* Calcineurin and Its Regulator Sra/DSCR1 Are Essential for Sleep in. *Journal of Neuroscience* **31**, 12759-12766 (2011).

40 Tomita, J. *et al.* Pan-neuronal knockdown of calcineurin reduces sleep in the fruit fly, Drosophila melanogaster. *Journal of Neuroscience* **31**, 13137-13146 (2011).

41 Yin, X. *et al.* Calcineurin governs baseline and homeostatic regulations of non-rapid

eye movement sleep in mice. *Proceedings of the National Academy of Sciences of the United States of America* **122** (2025).

42 Yu, J. J. *et al.* Calcineurin: An essential regulator of sleep revealed by biochemical, chemical biological, and genetic approaches. *Cell Chem Biol* **32** (2025).

43 Wang, G. D. *et al.* Somatic Genetics Analysis of Sleep in Adult Mice. *Journal of Neuroscience* **42**, 5617-5640 (2022).

44 Liu, S., Liu, Q., Tabuchi, M. & Wu, M. N. Sleep Drive Is Encoded by Neural Plastic Changes in a Dedicated Circuit. *Cell* **165**, 1347-1360 (2016).

45 Pinto, M. J. *et al.* Microglial TNFα orchestrates protein phosphorylation in the cortex during the sleep period and controls homeostatic sleep. *Embo Journal* **42** (2023).

46 Gay, S. M. *et al.* Developing forebrain synapses are uniquely vulnerable to sleep loss. *Proc Natl Acad Sci U S A* **121**, e2407533121 (2024).

47 Yu, F. H. *et al.* Reduced sodium current in GABAergic interneurons in a mouse model of severe myoclonic epilepsy in infancy. *Nature Neuroscience* **9**, 1142-1149 (2006).

48 Han, S. *et al.* Autistic-like behaviour in Scn1a+/- mice and rescue by enhanced GABA-mediated neurotransmission. *Nature* **489**, 385-390 (2012).

49 Hu, W. *et al.* Distinct contributions of Na(v)1.6 and Na(v)1.2 in action potential initiation and backpropagation. *Nat Neurosci* **12**, 996-1002 (2009).

50 Ma, Z. X. *et al.* Deficiency of autism-related gene in mice disrupts sleep patterns and circadian rhythms. *Neurobiology of Disease* **168** (2022).

51 Tamura, S. *et al.* CRISPR activation for SCN2A-related neurodevelopmental disorders. *Nature* (2025).

52 Park, K. S., Mohapatra, D. P., Misonou, H. & Trimmer, J. S. Graded regulation of the Kv2.1 potassium channel by variable phosphorylation. *Science* **313**, 976-979 (2006).

53 Planells-Cases, R. *et al.* Neuronal death and perinatal lethality in voltage-gated sodium channel α-deficient mice. *Biophysical journal* **78**, 2878-2891 (2000).

54 Shi, Y. Y. & Wang, G. F. Protocol to study microcircuits in the medial entorhinal cortex in mice using multiple patch-clamp recordings and morphological reconstruction. *STAR protocols* **5** (2024).

55 Wang, G. F. *et al.* An optogenetics- and imaging-assisted simultaneous multiple patch-clamp recording system for decoding complex neural circuits. *Nat Protoc* **10** (2015).

56 Deverman, B. E. *et al.* Cre-dependent selection yields AAV variants for widespread gene transfer to the adult brain. *Nature Biotechnology* **34**, 204-+ (2016).

57 Bjorness, T. E., Kelly, C. L., Gao, T. S., Poffenberger, V. & Greene, R. W. Control and function of the homeostatic sleep response by adenosine A1 receptors. *Journal of Neuroscience* **29**, 1267-1276 (2009).

58 Tomita, J., Ueno, T., Mitsuyoshi, M., Kume, S. & Kume, K. The NMDA Receptor Promotes Sleep in the Fruit Fly, Drosophila melanogaster. *PLoS One* **10**, e0128101 (2015).

59 Holst, S. C. *et al.* Cerebral mGluR5 availability contributes to elevated sleep need and behavioral adjustment after sleep deprivation. *eLife* **6** (2017).

60 Lin, L. *et al.* The sleep disorder canine narcolepsy is caused by a mutation in the hypocretin (orexin) receptor 2 gene. *Cell* **98**, 365-376 (1999).

61 Chemelli, R. M. *et al.* Narcolepsy in orexin knockout mice: molecular genetics of

sleep regulation. *Cell* **98**, 437-451 (1999).

62 Ma, W. X. *et al.* Adenosine and P1 receptors: Key targets in the regulation of sleep, torpor, and hibernation. *Frontiers in pharmacology* **14**, 1098976 (2023).

63 Peng, W. *et al.* Regulation of sleep homeostasis mediator adenosine by basal forebrain glutamatergic neurons. *Science* **369** (2020).

64 Liu, Z. Y. *et al.* LKB1 is physiologically required for sleep from Drosophila melanogaster to the Mus musculus. *Genetics* **221** (2022).

65 Siwek, M. E. *et al.* The Ca2.3 R-type voltage-gated Ca channel in mouse sleep architecture. *Sleep* **37**, 1721-1721 (2014).

66 Douglas, C. L. *et al.* Sleep in Kcna2 knockout mice. *BMC biology* **5** (2007).

67 Suzuki, A., Yanagisawa, M. & Greene, R. W. Loss of Arc attenuates the behavioral and molecular responses for sleep homeostasis in mice. *Proceedings of the National Academy of Sciences of the United States of America* **117**, 10547-10553 (2020).

68 Zhang, Y. *et al.* Voltage Gated Ion Channels and Sleep. *J Membrane Biol* **257**, 269-280 (2024).

69 Humphrey, S. J., James, D. E. & Mann, M. Protein Phosphorylation: A Major Switch Mechanism for Metabolic Regulation. *Trends Endocrinol. Metab.* **26**, 676-687 (2015).

70 Johnson, J. L. *et al.* An atlas of substrate specificities for the human serine/threonine kinome. *Nature* **613**, 759-766 (2023).

71 Chen, M. M. *et al.* GPS 6.0: an updated server for prediction of kinase-specific phosphorylation sites in proteins. *Nucleic acids research* **51**, W243-W250 (2023).

72 Rossie, S., Gordon, D. & Catterall, W. A. Identification of an Intracellular Domain of the Sodium-Channel Having Multiple Camp-Dependent Phosphorylation Sites. *Journal of Biological Chemistry* **262**, 17530-17535 (1987).

73 Wang, Y. *et al.* Isoform-selective disruption of AKAP-localized PKA using hydrocarbon stapled peptides. *ACS chemical biology* **9**, 635-642 (2014).

74 Liu, Y., Qin, N., Reitz, T., Wang, Y. & Flores, C. M. Inhibition of the rat brain sodium channel Nav1.2 after prolonged exposure to gabapentin. *Epilepsy research* **70**, 263-268 (2006).

75 Ehlers, C. L., Sanchez-Alavez, M. & Wills, D. Effect of gabapentin on sleep and delta and theta EEG power in adult rats exposed to chronic intermittent ethanol vapor and protracted withdrawal during adolescence. *Psychopharmacology* **235**, 1783-1791 (2018).

76 Lo, H. S. *et al.* Treatment Effects of Gabapentin for Primary Insomnia. *Clin Neuropharmacol* **33**, 84-90 (2010).

77 Shen, Y. N., Li, W., Ma, M. & Jiang, W. H. Efficacy and Safety of Gabapentin in Improving Sleep Quality of Patients with Sensory Nervous System Diseases: A Meta-Analysis. *Altern Ther Health M* **29**, 380-385 (2023).

78 Susantitapong, K., Dilokpattanamongkol, P., Sutherasan, Y., Liamsombut, S. & Suthisisang, C. Effects of gabapentin on slow-wave sleep period in critically ill adult patients: A randomized controlled trial. *Cts-Clin Transl Sci* **17** (2024).

79 Huber, R., Ghilardi, M. F., Massimini, M. & Tononi, G. Local sleep and learning. *Nature* **430**, 78-81 (2004).

80 Quintela-López, T., Shiina, H. & Attwell, D. Neuronal energy use and brain evolution. *Curr Biol* **32**, R650-r655 (2022).

81 Lee, C., Etchegaray, J. P., Cagampang, F. R. A., Loudon, A. S. I. & Reppert, S. M. Posttranslational mechanisms regulate the mammalian circadian clock. *Cell* **107**, 855-867 (2001).

82 Lee, H. M. *et al.* The period of the circadian oscillator is primarily determined by the balance between casein kinase 1 and protein phosphatase 1. *Proceedings of the National Academy of Sciences of the United States of America* **108**, 16451-16456 (2011).

83 Jolley, C. C., Ode, K. L. & Ueda, H. R. A Design Principle for a Posttranslational Biochemical Oscillator. *Cell reports* **2**, 938-950 (2012).

84 Nakajima, M. *et al.* Reconstitution of circadian oscillation of cyanobacterial KaiC phosphorylation in vitro. *Science* **308**, 414-415 (2005).

85 Liao, M. *et al.* The P-loop NTPase RUVBL2 is a conserved clock component across eukaryotes. *Nature* **642**, 165-173 (2025).

86 Asano, F. *et al.* SIK3-HDAC4 in the suprachiasmatic nucleus regulates the timing of arousal at the dark onset and circadian period in mice. *Proceedings of the National Academy of Sciences of the United States of America* **120** (2023).

87 Wang, Z. *et al.* Orexin/hypocretin activates mTOR complex 1 (mTORC1) via an Erk/Akt-independent and calcium-stimulated lysosome v-ATPase pathway. *The Journal of biological chemistry* **289**, 31950-31959 (2014).

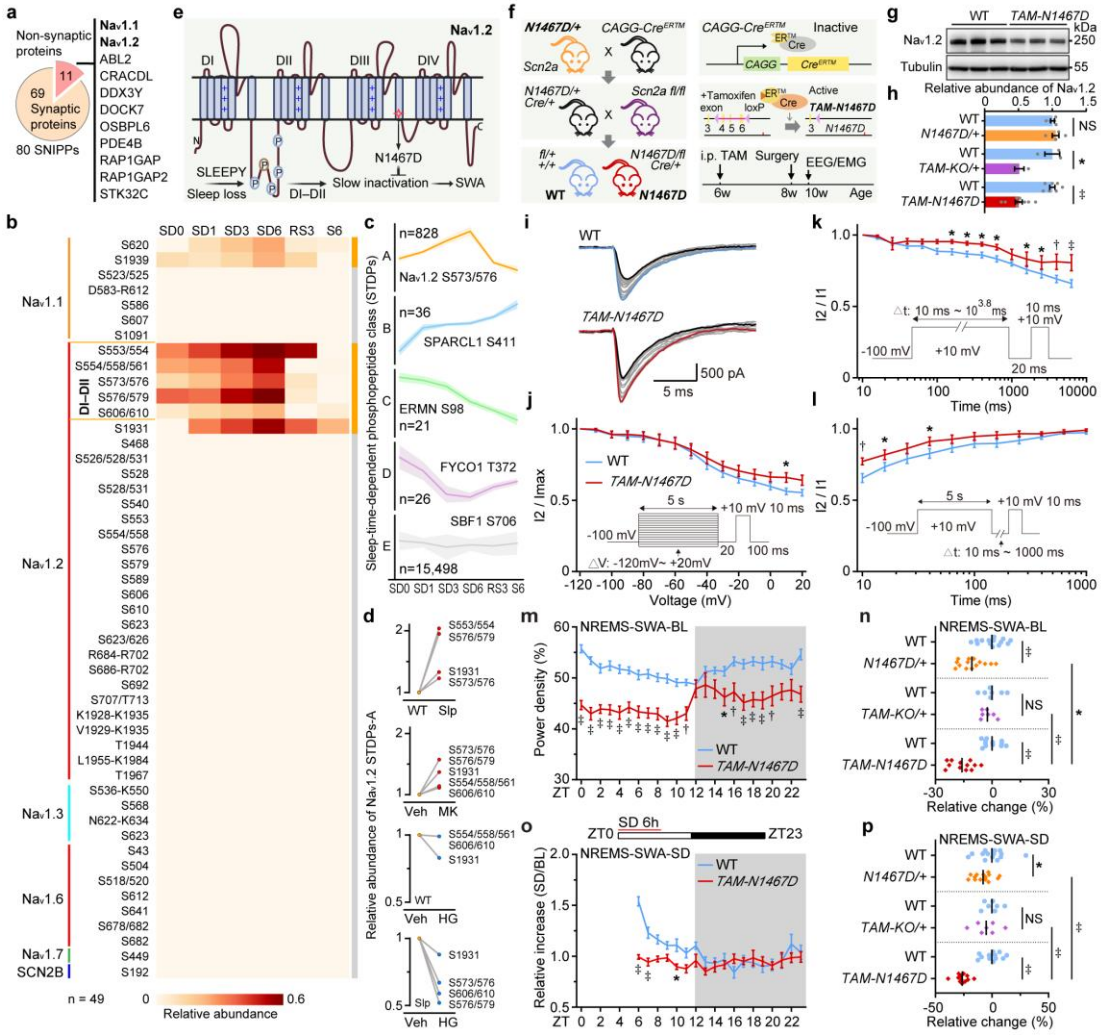

Fig. 1. Impaired slow inactivation of $Na_v1.2$ attenuates SWA of NREMS.

a, A summary of non-synaptic SNIPPs.

b, Temporal profile and classification of Na^+ channel family phosphopeptides.

c, Representative phosphopeptides for STDPs A-E.

d, Analysis of mean abundance of $Na_v1.2$ STDPs-A in 4 altered sleep need models.

e, A schematic of the domain structure of $Na_v1.2$.

f, Schematic of constructs for tamoxifen-inducible *Scn2a*^{N1467D} homozygous mice (*TAM-N1467D*).

g, h Representative immunoblots (**g**) and quantitative analysis (**h**) for the abundance of brain $Na_v1.2$. WT (n=5) vs. *N1467D/+* (n=5), WT (n=3) vs. *TAM-KO/+* (n=3), and WT (n=7) vs. *TAM-N1467D* (n=9).

i-l, Measurements of slow inactivation in layer 5 neurons from WT and *TAM-N1467D* mice. Representative current traces (**i,** 15 vs. 15), voltage dependence (**j,** 17 vs. 16), onset (**k,** 10 vs. 7), and recovery (**l,** 17 vs. 9) of slow inactivation. The insets in (**j-l**) display voltage protocols. **m-p,** Analyses baseline (**m, n**) and rebound NREMS-SWA (**o, p**). WT (n=14) vs. *N1467D/+* (n=14), WT (n=7) vs. *TAM-KO/+* (n=7), and WT (n=12) vs. *TAM-N1467D* (n=12). Data shown as mean ± s.e.m. Two-way ANOVA with Sidak's test (**m**, **o**); two-way ANOVA with Fisher's LSD test (**j-l**); Ordinary one-way ANOVA with Fisher's LSD test (**n, p**) and two-tailed unpaired *t*-test (**h**). * $P < 0.05$; † $P < 0.01$; ‡ $P < 0.001$; NS, not significant, $P > 0.05$.

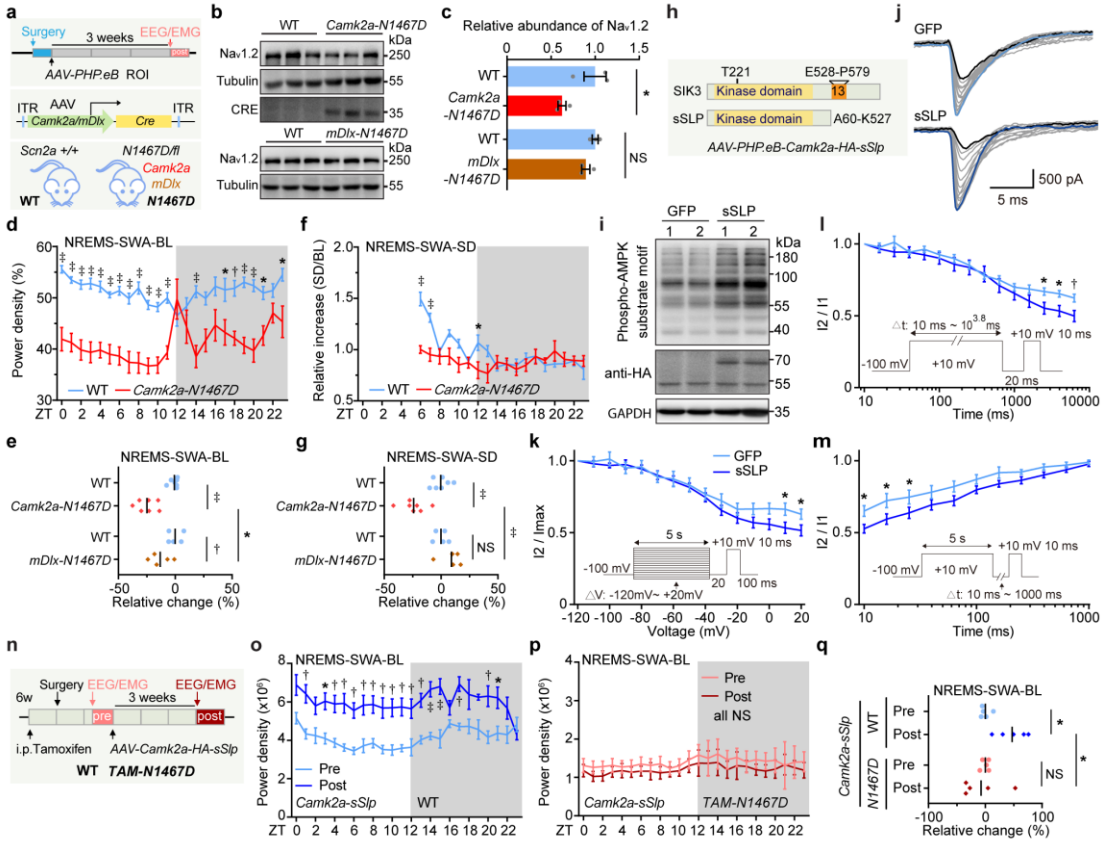

Fig. 2. $Na_v1.2$ functions in excitatory neurons and acts downstream of SLEEPY kinase.

a, Schematic of adult-brain-chimeric knockout of *Scn2a* by retro-orbital injection of AAV-PHP.eB into *Scn2a*$^{N1467D/fl}$ mice.

b, c Representative immunoblots (**b**) and quantitative analysis (**c**) for the abundance of brain $Na_v1.2$. WT (n=3) vs. *Camk2a-N1467D* (n=3) and WT (n=3) vs. *mDlx-N1467D* (n=3).

d-g, Analyses baseline (**d, e**) and rebound NREMS-SWA (**f, g**). WT (n=7) vs. *Camk2a-N1467D* (n=7), WT (n=5) vs. *mDlx-N1467D* (n=5).

h, Schematic diagram of the protein structure of truncated SIK3 protein (sSLP).

i, Immunoblotting of brain lysates from mice injected with AAV expressing *HA-sSlp* with AMPK phosphorylation substrate motif antibody.

j-m, Measurements of slow inactivation in layer 5 neurons from GFP and sSLP mice. Representative current traces (**j,** 15 vs. 15), voltage dependence (**k,** 38 vs. 25), onset (**l,** 33 vs. 26), and recovery (**m,** 33 vs. 18) of slow inactivation.

n, A schematic for sSLP expression in WT and *TAM-N1467D* mice.

o-q, Circadian (**o, p**) and quantitative (**q**) analyses of baseline NREMS-SWA before (pre) and after (post) AAV-*Camk2a-HA-sSlp* injection in WT (**o**, n=5) and *TAM-N1467D* (**p**, n=5) mice. Data shown as mean ± s.e.m. Two-way ANOVA with Sidak's test (**d, f, o-p**); two-way ANOVA with Fisher's LSD test (**k-m**); Ordinary one-way ANOVA with Fisher's LSD test (**e, g**); two-tailed unpaired *t*-test (**c, q**) and two-tailed unpaired *t*-test (**q**). * $P < 0.05$; † $P < 0.01$‡ $P < 0.001$; NS, not significant, $P > 0.05$.

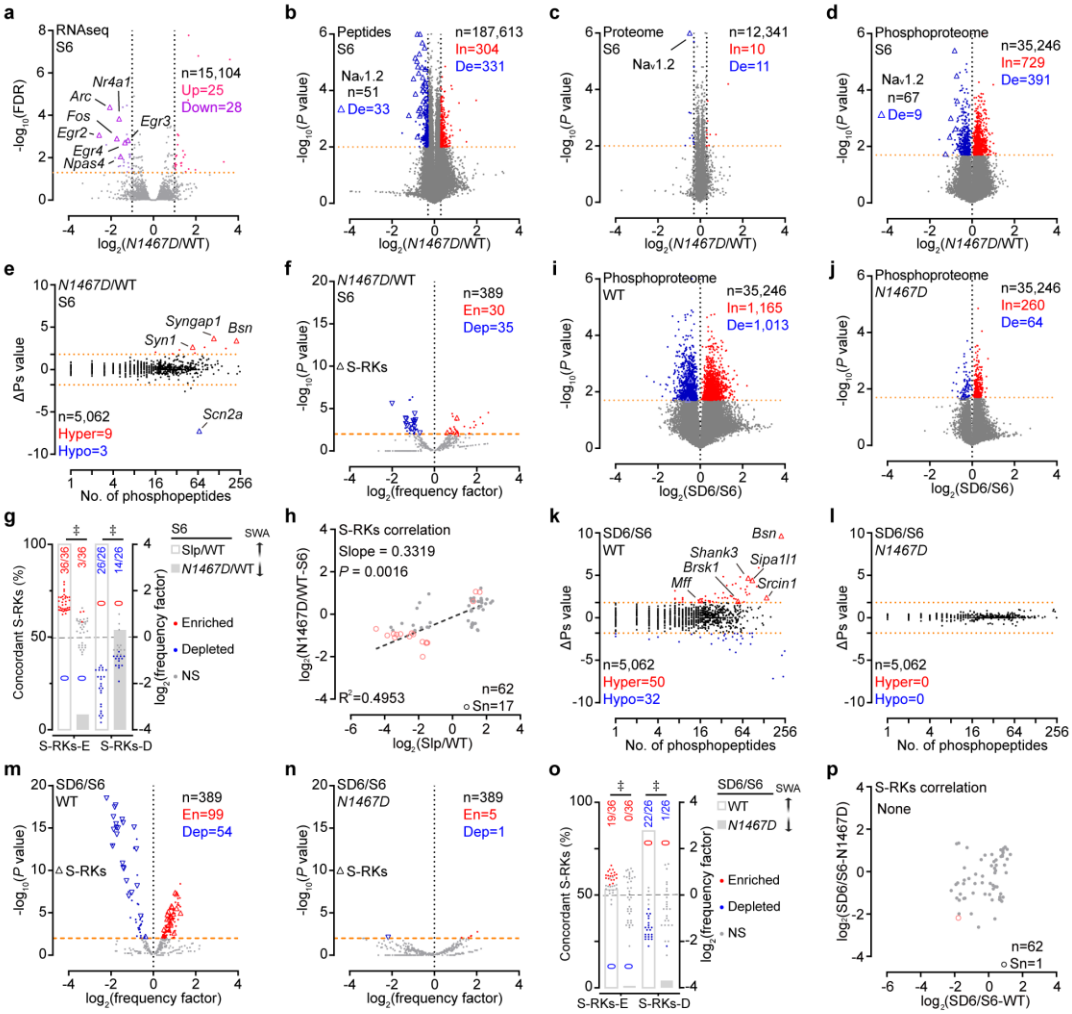

Fig.3. Na$_V$1.2 gates sleep-associated signaling pathways in brain.

a-c Volcano plots illustrating changes in RNA expression (**a**), peptide abundance (**b**), and protein abundance (**c**) in the N1467D/WT (S6) comparison. Immediate early genes are labeled (**a**).

d-f, Phosphoproteomic analysis of the *N1467D*/WT (S6) comparison in phosphopeptide changes (**d**), global ΔPs of phosphoproteins (**e**), global kinase motif enrichment (**f**).

g, Percentage and frequency factor of S-RKs-E (n=36) and S-RKs-D (n=26) in the Slp/WT and N1467D/WT (S6) comparison. The fraction of concordant S-RKs was marked at the top of each column.

h, Correlation analysis of S-RKs significantly enriched or depleted in both comparisons. Percentage and correlation analyses of S-RKs revealed positive concordance when comparing

the Slp/WT with SD6/RS3 comparisons, negative concordance in the HG/Veh (Slp) comparison, and no concordance in the N1467D/WT comparison. Thus, changes in S-RKs activity paralleled changes in NREMS-SWA in the validated "altered sleep need" models, but this parallelism was absent in the N1467D/WT comparison—indicating specifically weaker coupling between S-RKs and SWA in N1467D mice.

i-p, Phosphoproteomic analysis of SD6/S6 (WT) and SD6/S6 (*N1467D*) comparisons in phosphopeptide changes (**i, j**), global ΔPs of phosphoproteins (**k, l**) global kinase motif enrichment (**m, n**), percentage and frequency factor of S-RKs (**o**), and correlation analysis of S-RKs (**p**).

Up, up-regulated; Down, down-regulated. In, increase; De, decrease. En, enriched; Dep, depleted. Hyper, hyperphosphorylated; Hypo, hypophosphorylated.

Dashed line represents -log10 (FDR) =1.3 on y-axis, and $|\log_2 FC|=1$ on x-axis(**a**).

Multiple unpaired t-test (*P* value) (**b-d**, **i, j**).

Dashed line represents ΔPs = ±1.8 (**e, k, l**).

Fisher's exact test was used for percentage analysis (**g, o**).

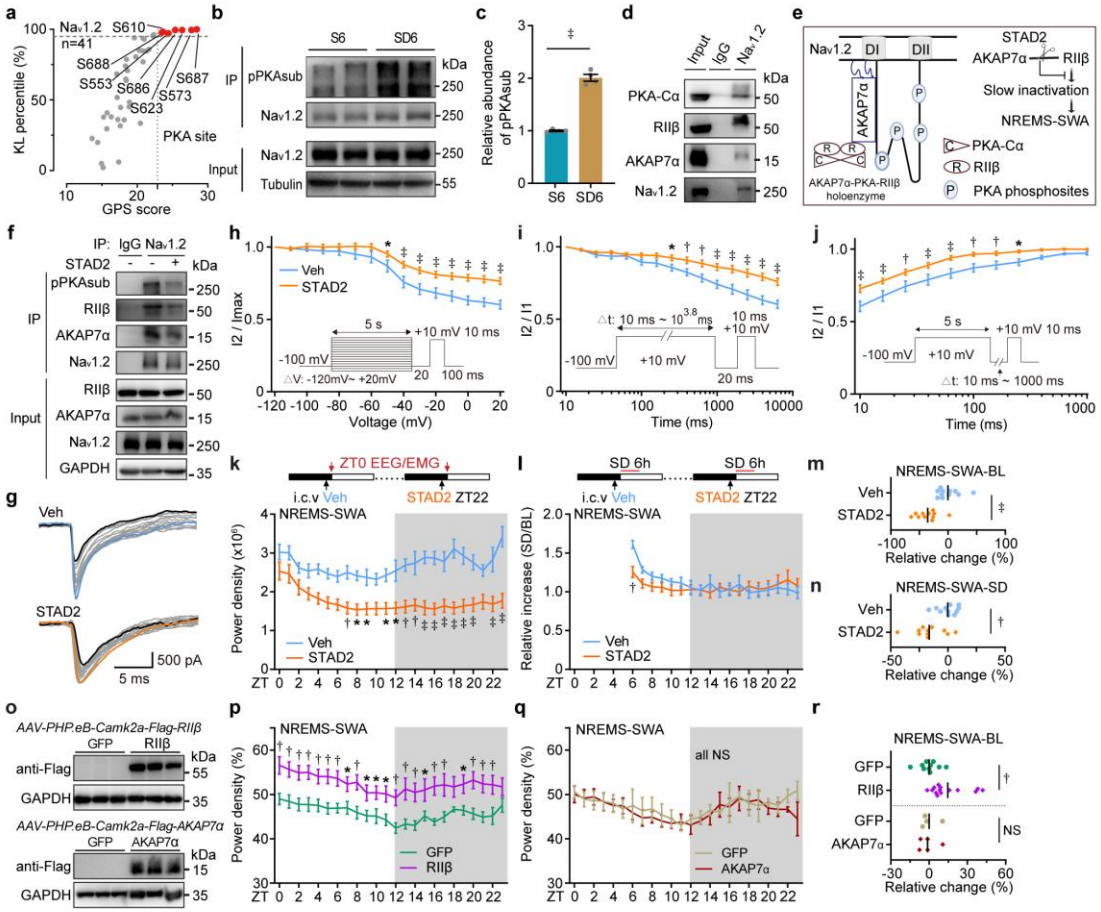

Fig. 4. The RIIβ-PKA holoenzyme promotes Na$_v$1.2 phosphorylation and sleep quality.

a, PKA substrate site prediction for Na$_v$1.2 (n=41) by Group-based Prediction System (GPS) and Kinase-Library (KL). Threshold (score = 22.8, percentile=95).

b, c Representative immunoblots (**b**) and quantitative analysis (**c**) for the abundance of PKA substrate motif (pPKAsub) in Na$_v$1.2 immunoprecipitates under S6 (n=4) and SD6 (n=4) conditions.

d-f, Co-IP analysis identifying Na$_v$1.2-associated proteins (**d**). Schematic illustration showing the interaction between PKA-Cα, RIIβ, AKAP7α and the DI–II loop of Na$_v$1.2, and STAD2 treatment effect (**e**). Co-IP analysis of Na$_v$1.2 following i.c.v. STAD2 treatment (**f**).

g-j, Measurements of slow inactivation in layer 5 neurons from mice injected with vehicle (Veh) and STAD2. Representative current traces (**g,** 15 vs. 15), voltage dependence (**h,** 16 vs. 30), onset (**i,** 13 vs. 26), and recovery (**j,** 16 vs. 23) of slow inactivation.

k-n, Analyses baseline (**k, m**) and rebound NREMS-SWA (**l, n**) injected with Veh and STAD2 (n=11).

o-r, Representative immunoblots (**o**), circadian (**p, q**) and quantitative (**r**) analyses of baseline NREMS-SWA for mice injected with AAV-*Camk2a* virus. GFP (n=10) vs. RIIβ (n=14); GFP (n=4) vs. AKAP7α (n=5).

Data shown as mean ± s.e.m. Two-way ANOVA with Fisher's LSD (**h-j, p**); two-way ANOVA with Sidak's test (**k-l, q**); two-tailed unpaired *t*-test (**c, r**) and two-tailed paired *t*-test (**m, n**). * $P < 0.05$; † $P < 0.01$; ‡ $P < 0.001$; NS, not significant, $P > 0.05$.

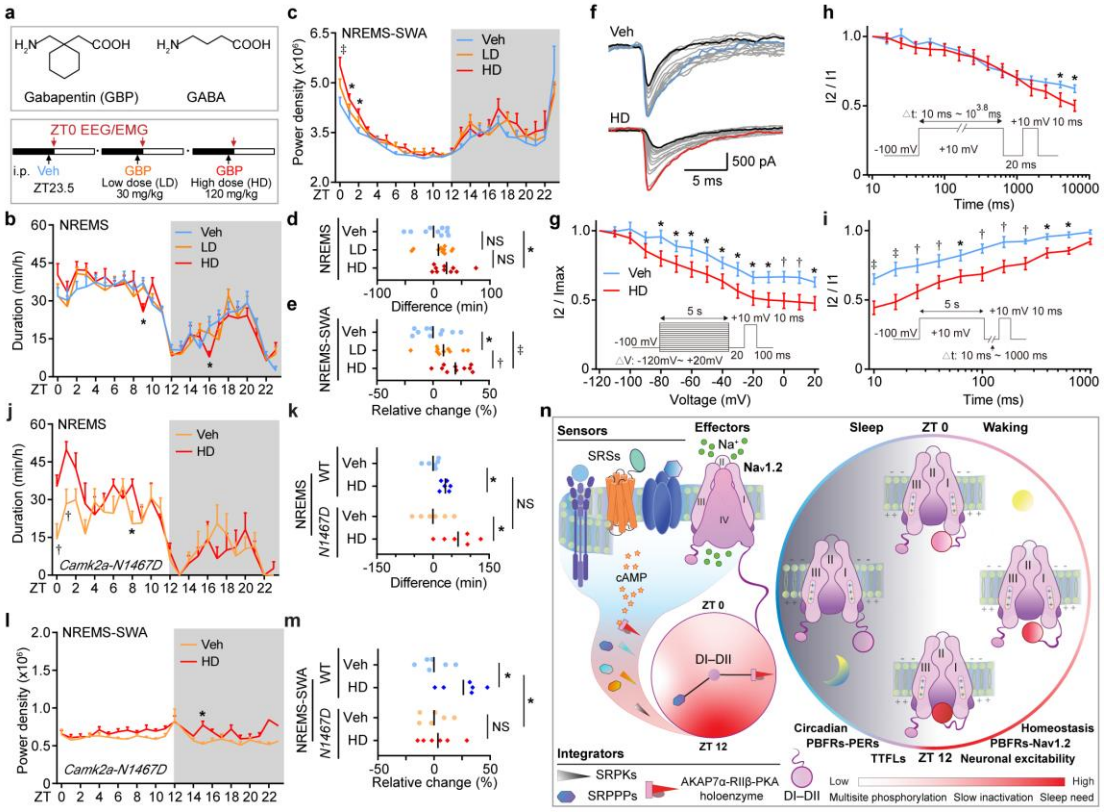

Fig. 5. Gabapentin improves sleep quality via $Na_v1.2$ in mice.

a, Chemical structure of gabapentin and schematic of the experimental protocol.

b-e, Circadian analyses of baseline NREMS (**b, d**) and NREMS-SWA (**c, e**) in mice i.p. injected with Veh or GBP (n=10).

f-i, Measurements of slow inactivation in layer 5 neurons from mice injected with Veh and HD-GBP (120 mg/kg). Representative current traces (**f,** 15 vs. 15), voltage dependence (**g,** 38 vs. 29), onset (**h,** 33 vs. 21), and recovery (**i,** 33 vs. 17) of slow inactivation.

j-m, Circadian (**j, l**) and quantitative (**k, m**) analyses of baseline NREMS and NREMS-SWA in WT (n=6) and *Camk2a-N1467D* (n=6) mice injected with Veh and HD-GBP.

n, Molecular model of the AKAP7α-RIIβ-PKA-$Na_v1.2$ complex forms a compact homeostatic oscillator to regulate sleep quality.

Data shown as mean ± s.e.m. Ordinary one-way ANOVA with Fisher's LSD (**d**); two-way ANOVA with Dunnett's test (**b-c**); two-way ANOVA with Fisher's LSD(**f-h**); two-way ANOVA with Sidak's test (**k**) and Wilcoxon matched-pairs test and Mann-Whitney test (**j, l**).

1089 * $P < 0.05$; † $P < 0.01$; ‡ $P < 0.001$; NS, not significant, $P > 0.05$.

1090

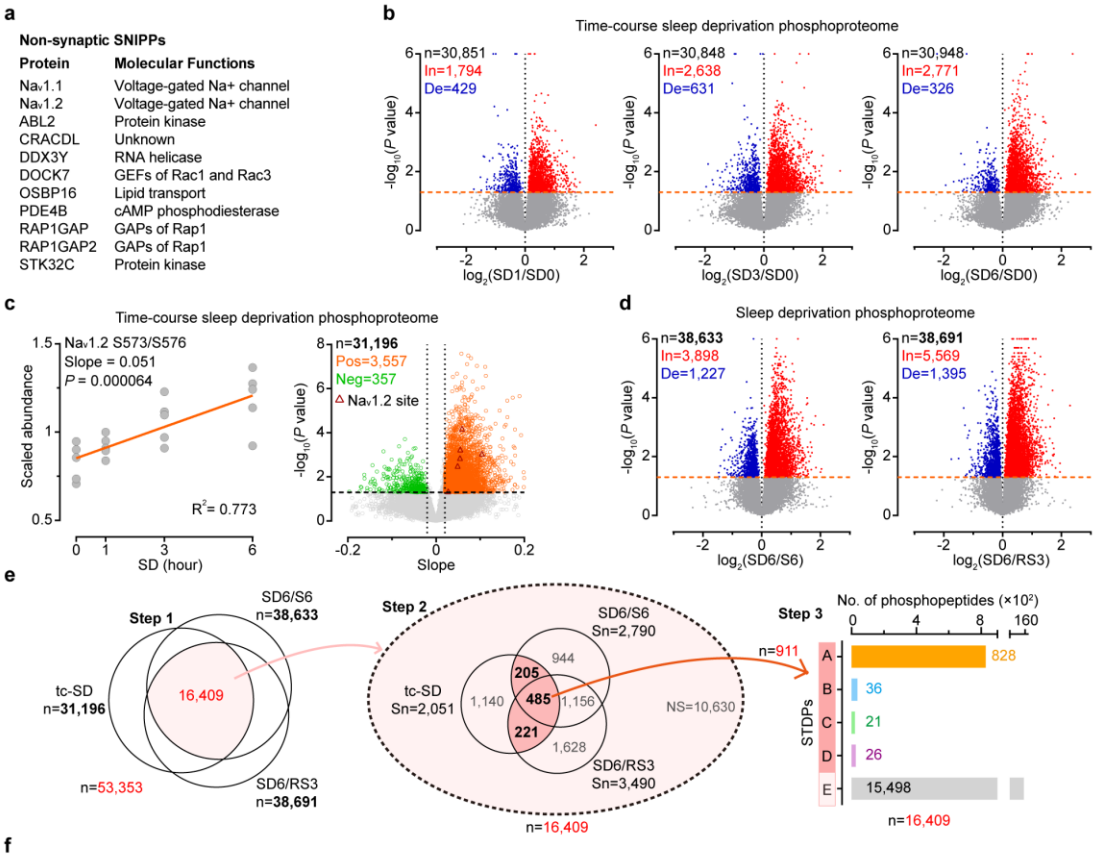

	Step1				Step2				Step3				
Mouse Protein	tc-SD	RS3	S6	Shared	tc-SD	RS3	S6	STDPs	A	B	C	D	E
Nav1.1	21	30	30	7	2	3	3	2	2	0	0	0	5
SCN1B	1	1	1	0	0	0	0	0	0	0	0	0	0
Nav1.2	62	61	61	29	9	11	12	6	**6**	0	0	0	23
SCN2B	3	4	4	1	0	0	0	0	0	0	0	0	1
Nav1.3	5	9	9	4	1	1	1	0	0	0	0	0	4
SCN3B	1	1	1	0	0	0	0	0	0	0	0	0	0
Nav1.4	1	0	0	0	0	0	0	0	0	0	0	0	0
SCN4B	1	1	1	0	0	0	0	0	0	0	0	0	0
Nav1.5	1	0	0	0	0	0	0	0	0	0	0	0	0
Nav2.3	1	2	2	0	0	0	0	0	0	0	0	0	0
Nav1.6	12	17	17	7	0	1	2	0	0	0	0	0	7
Nav1.7	3	3	3	1	0	1	0	0	0	0	0	0	1
Total	112	129	129	**49**	12	17	18	8	8	0	0	0	41

Extended Data Fig. 1 | Analysis approach for the classification of sleep-time-dependent phosphopeptides.

a, Summary of the functions of non-synaptic SNIPPs.

b-d, Phosphoproteomic analysis of time-course sleep deprivation (tc-SD, **b**) and sleep deprivation (SD, **d**) models. Representative ($Na_V1.2$ S573/S576, left) and global linear regression analysis of tc-SD phosphoproteome (right) (**c**).

e, Overlapping analysis of two SD models to identify sleep-time-dependent phosphopeptides classes A-E.

f, Summary of phosphopeptides number of 12 Na^+ channel family members.

1101 Data shown as correlation (r) and regression slope with two-tailed t-tests(**d**)

1102

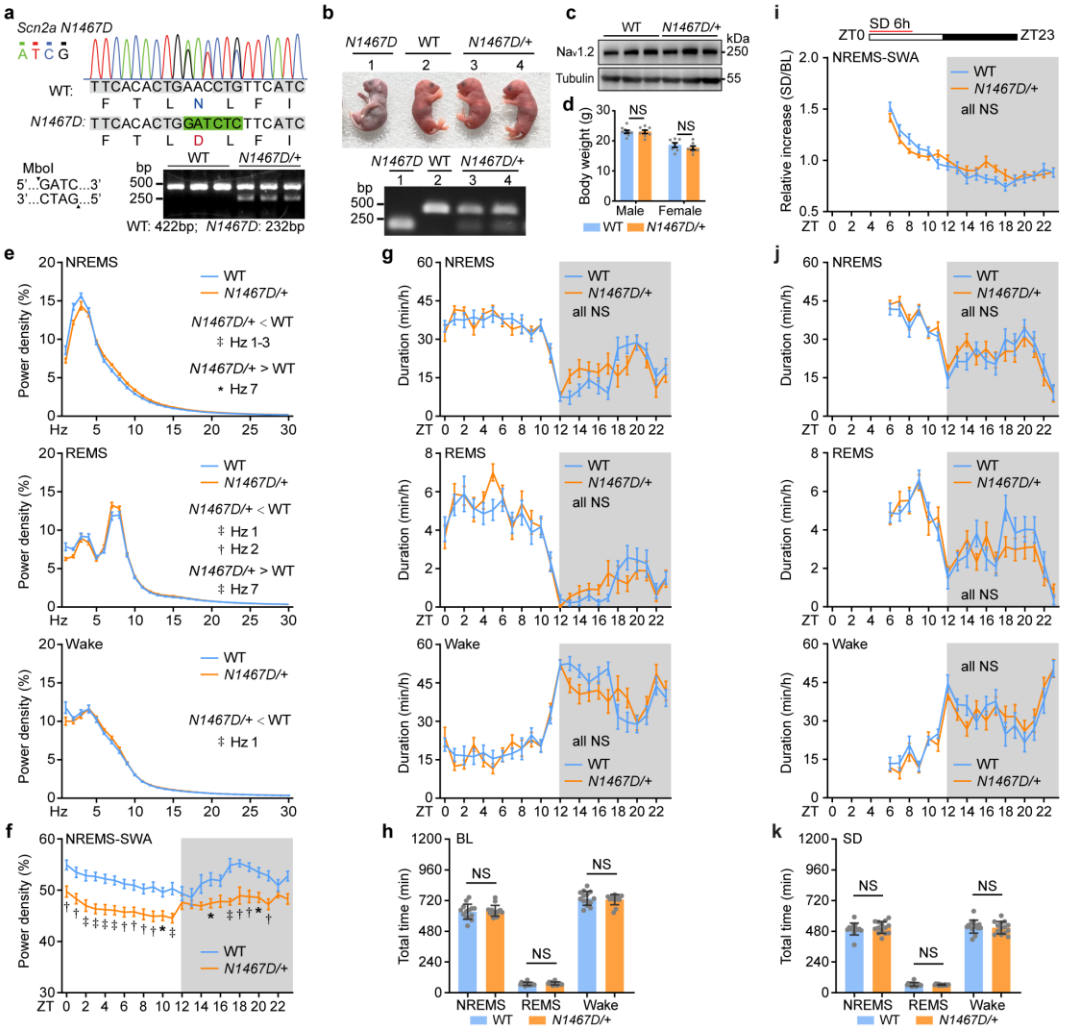

Extended Data Fig. 2 | Generation and characterization of *Scn2a*^{N1467D} mutant mice.

a, Direct sequencing, genotyping designs, and RT-PCR of the N1467D/+ mutant mouse.

b, Postnatal mortality of *N1467D* mice and genotyping results.

c, Representative immunoblots for the abundance of brain $Na_v1.2$ of WT and *N1467D/+* mice.

d, Comparison of body weight between WT (n=9 male, 7 female) and *N1467D/+* (n= 8 male, 7 female) mice.

e-k, Sleep analyses for WT (n=14) and *N1467D/+* mice (n=14). Relative EEG power spectra (**e**), baseline NREMS-SWA (**f**), hourly (**g**) and total time (**h**) for NREMS, REMS and Wake. Rebound NREMS-SWA (**i**), hourly (**j**) and total time (**k**) for NREMS, REMS and Wake after 6 h sleep deprivation.

Data shown as mean ± s.e.m. Two-way ANOVA with Sidak's test (**e-g**, **i-j**) and two-tailed unpaired t-test (**d**, **h**, **k**). * $P < 0.05$; † $P < 0.01$; ‡ $P < 0.001$; NS, not significant, $P > 0.05$.

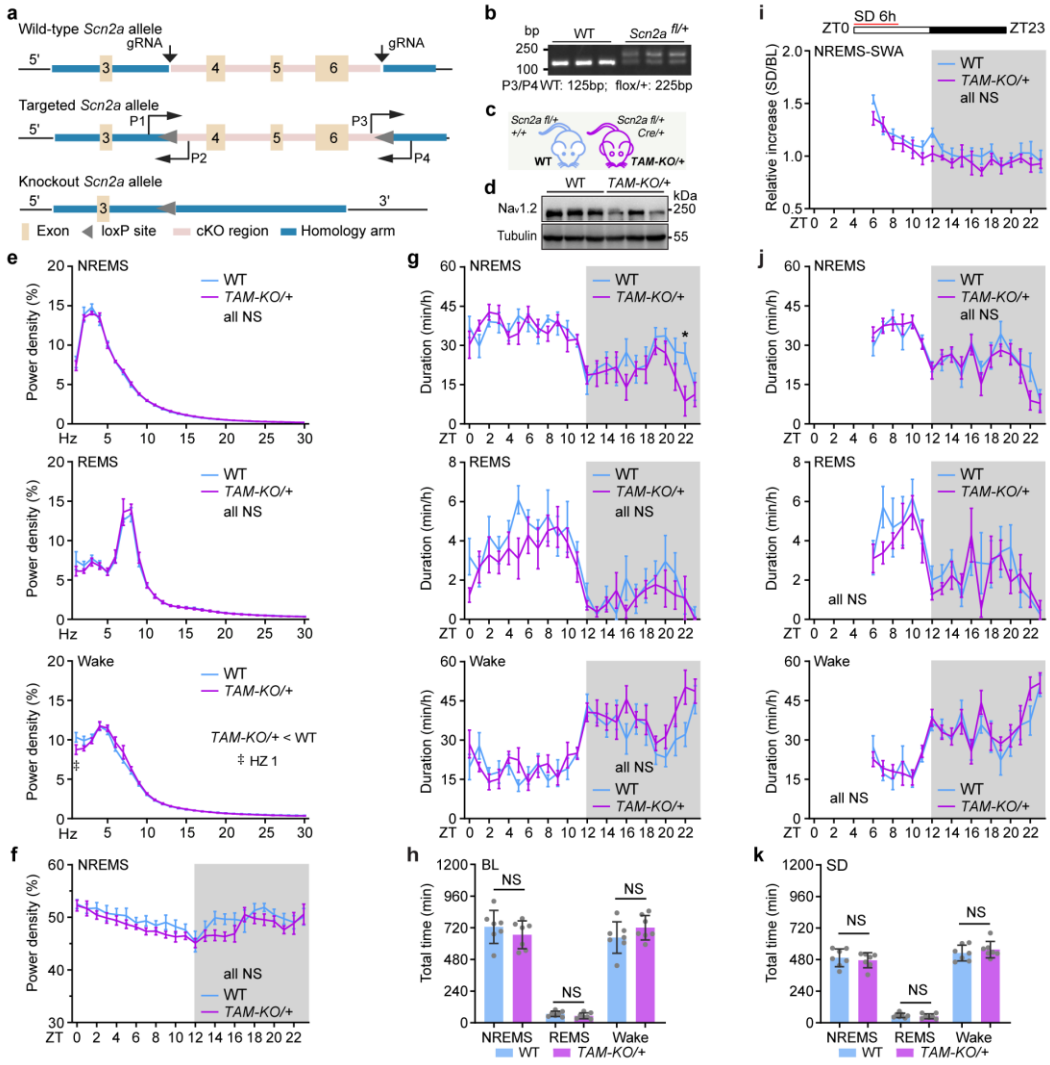

Extended Data Fig. 3 | Sleep analysis of *TAM-KO/+* mice.

a-d, Schematic of the gene editing design (**a**), genotyping (**b**), breeding strategy (**c**) and immunoblotting of $Na_v1.2$ in brain lysates from WT and *TAM-KO/+* mice (**d**)

e-k, Sleep analyses for WT (n=7) and *TAM-KO/+* mice (n=7). Relative EEG power spectra (**e**), baseline NREMS-SWA (**f**), hourly (**g**) and total time (**h**) for NREMS, REMS and Wake. Rebound NREMS-SWA (**i**), hourly (**j**) and total time (**k**) for NREMS, REMS and Wake after 6 h sleep deprivation.

Data shown as mean ± s.e.m. Two-way ANOVA with Sidak's test (**e-g, i-j**) and two-tailed unpaired t-test (**h**, **k**). * $P < 0.05$; † $P < 0.01$; ‡ $P < 0.001$; NS, not significant, $P > 0.05$.

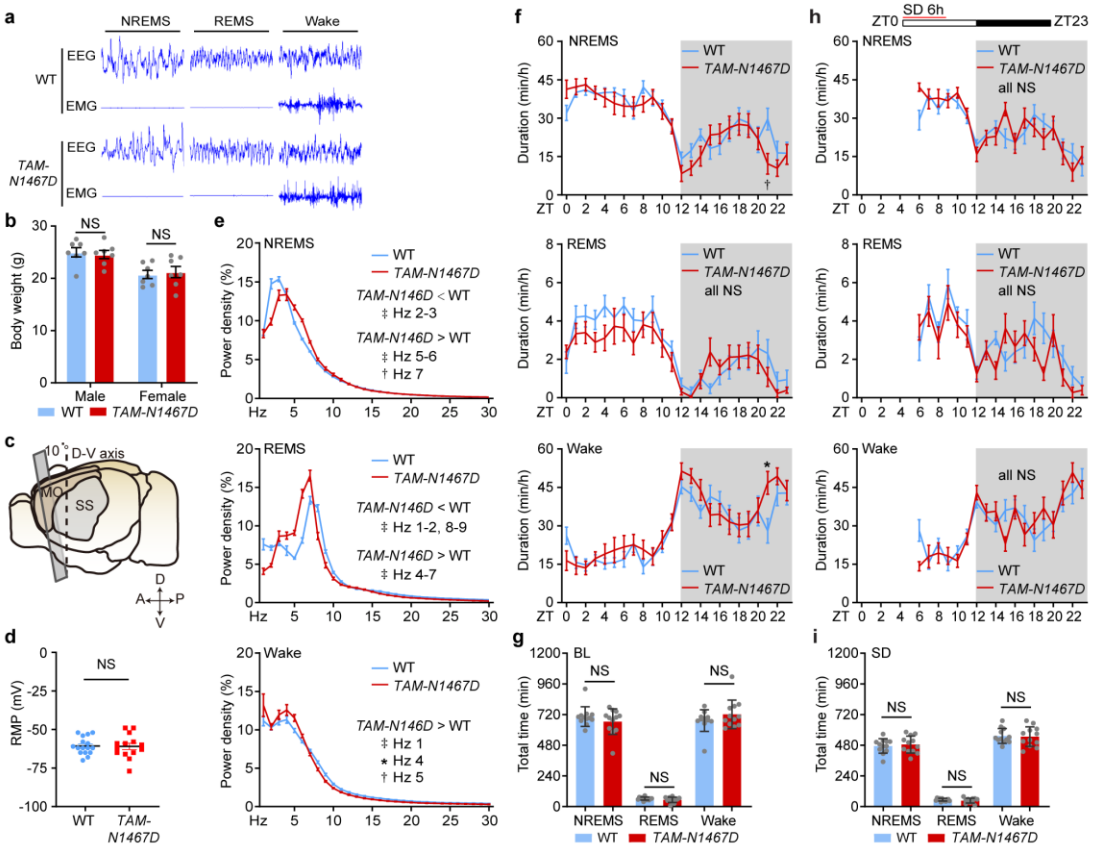

Extended Data Fig. 4 | Sleep analysis of *TAM-N1467D* mice.

a, Representative 8-s EEG and EMG for NREMS, REMS and Wake.

b, Comparison of body weight between WT (n=7 male, 7 female) and *TAM-N1467D* (n= 7 male, 7 female) mice.

c, Schematic of brain slice sampling. Slicing plane is tilted forward by 10°. MO, the motor cortex; SS, the somatosensory cortex.

d, Comparison of resting membrane potential (RMP) of neurons from WT (n=14) and *TAM-N1467D* (n=16) mice.

e-i, Sleep analyses for WT (n=12) and *TAM-N1467D* mice (n=12). Relative EEG power spectra (**e**), hourly (**f**) and total time (**g**) for NREMS, REMS and Wake. Hourly (**h**) and total time (**i**) for NREMS, REMS and Wake after 6 h sleep deprivation.

Data shown as mean ± s.e.m. Two-way ANOVA with Sidak's test (**e**, **f**, **h**) and two-tailed unpaired t-test (**b**, **d, g, i**). * $P < 0.05$; † $P < 0.01$; ‡ $P < 0.001$; NS, not significant, $P > 0.05$.

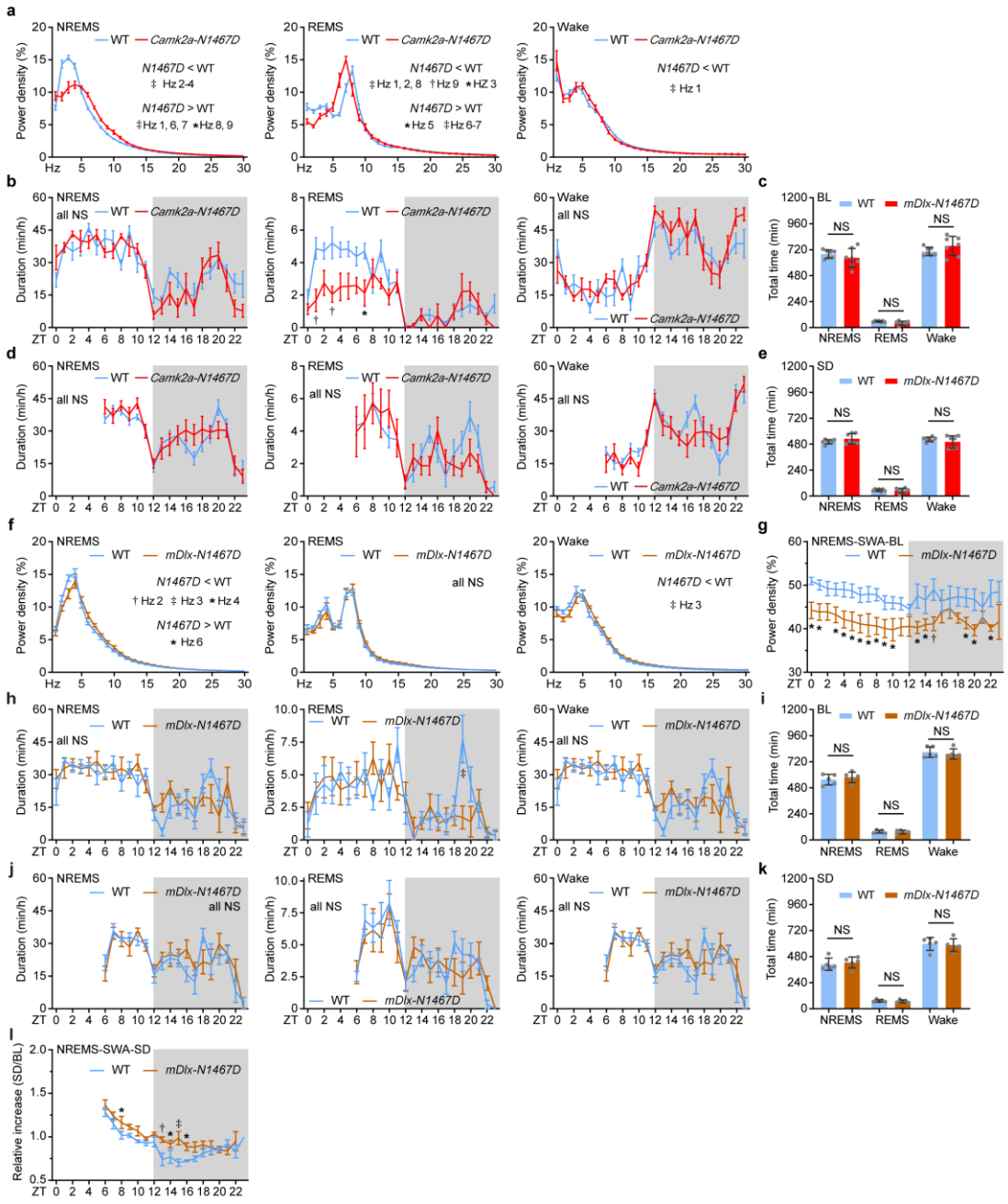

Extended Data Fig. 5 | Sleep analysis of *Camk2a-N1467D* and *mDlx-N1467D* mice.

a-e, Sleep analyses for WT (n=7) and *Camk2a-N1467D* mice (n=7). Relative EEG power spectra (**a**), hourly (**b**) and total time (**c**) for NREMS, REMS and Wake. Hourly (**d**) and total time (**e**) for NREMS, REMS and Wake after 6 h sleep deprivation.

f-i, Sleep analyses for WT (n=5) and *mDlx-N1467D* mice (n=5). Relative EEG power spectra (**f**), baseline NREMS-SWA (**g**), hourly (**h**) and total time (**i**) for NREMS, REMS and Wake. Hourly (**j**) and total time (**k**) for NREMS, REMS and Wake, and rebound NREMS-SWA (**l**)

after 6 h sleep deprivation.

Data shown as mean ± s.e.m. Two-way ANOVA with Sidak's test (**a-b**, **d**, **f-h**, **j, l**); RM one-way ANOVA with Fisher's LSD (**m**) and two-tailed unpaired t-test (**c**, **e**, **i, k**). * $P < 0.05$; † $P < 0.01$; ‡ $P < 0.001$; NS, not significant, $P > 0.05$.

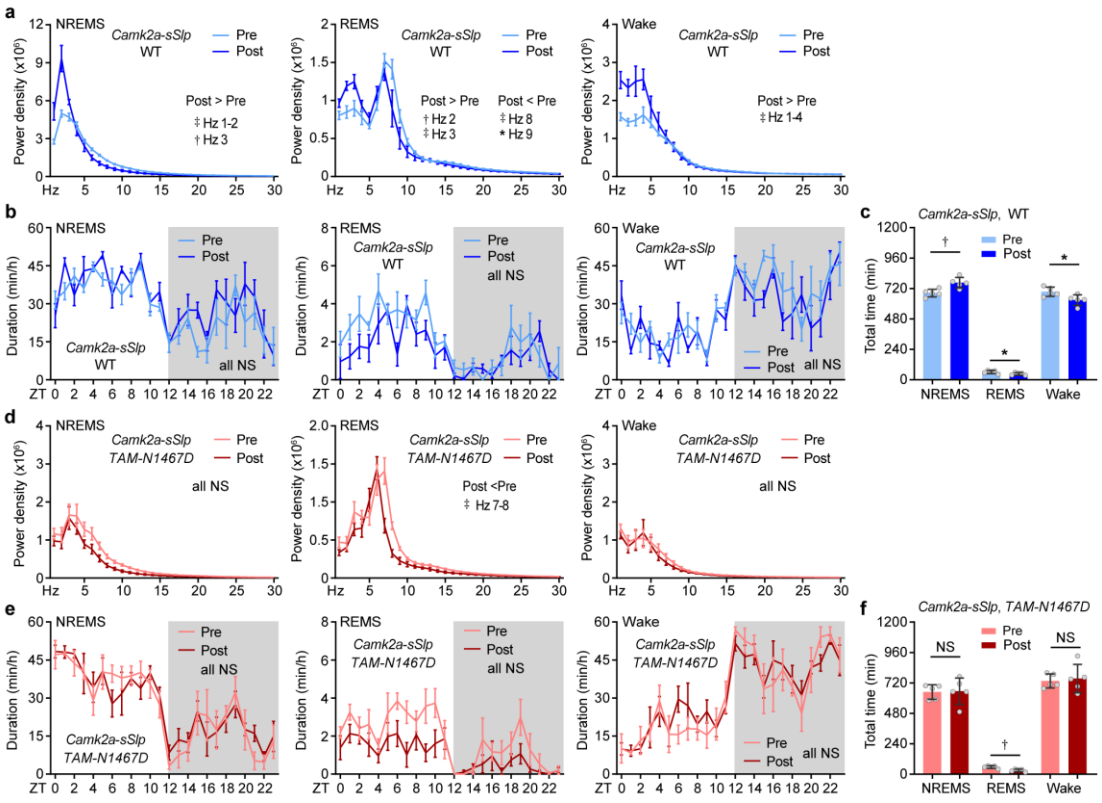

Extended Data Fig. 6 | Sleep analysis of WT and *TAM-N1467D* mice expressed with sSLP.

a-c, Sleep analyses for WT (n=5) mice expressed with sSLP. EEG power spectra (**a**), hourly (**b**) and total time (**c**) for NREMS, REMS and Wake.

d-f, Sleep analyses for *TAM-N1467D* (n=5) mice expressed with sSLP. EEG power spectra (**d**), hourly (**e**) and total time (**f**) for NREMS, REMS and Wake.

Data shown as mean ± s.e.m. Two-way ANOVA with Sidak's test (**a**-**b**, **e**) and two-tailed paired *t*-test (**c**, **f**). * $P < 0.05$; † $P < 0.01$; ‡ $P < 0.001$; NS, not significant, $P > 0.05$.

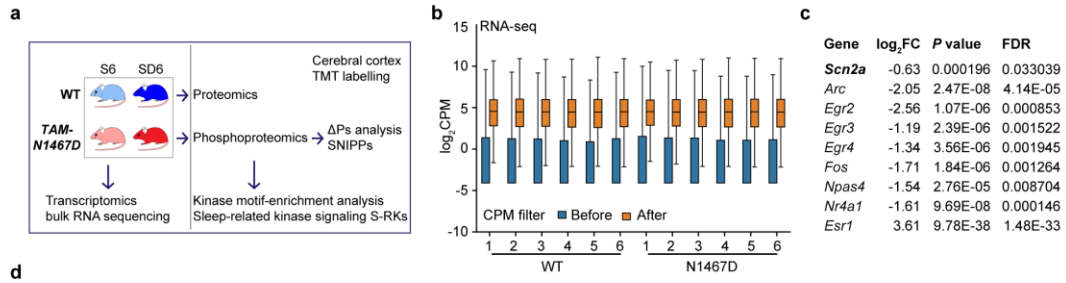

c

Gene	log_2FC	*P* value	FDR
Scn2a	-0.63	0.000196	0.033039
Arc	-2.05	2.47E-08	4.14E-05
Egr2	-2.56	1.07E-06	0.000853
Egr3	-1.19	2.39E-06	0.001522
Egr4	-1.34	3.56E-06	0.001945
Fos	-1.71	1.84E-06	0.001264
Npas4	-1.54	2.76E-05	0.008704
Nr4a1	-1.61	9.69E-08	0.000146
Esr1	3.61	9.78E-38	1.48E-33

d

Up-regulated genes

Gene	Protein and function
Adamts2	A disintegrin and metalloproteinase with thrombospondin motifs 2, cleaves the propeptides of type I and II collagen prior to fibril assembly
Aloxe3	Hydroperoxide isomerase ALOXE3, plays a crucial role in the synthesis of corneocytes lipid envelope
Apaf1	Apoptotic protease-activating factor 1, activates caspase-3 and apoptosis
Atg9b	Autophagy-related protein 9B, phospholipid scramblase involved in autophagy
Cd180	CD180 antigen, mediates the innate immune response
Cdkl4	Cyclin-dependent kinase-like 4, unknown
Crym	Ketimine reductase mu-crystallin, catalyzes the NAD(P)H-dependent reduction
Dio3	Thyroxine 5-deiodinase, thyroid hormones activation and inactivation by deiodination
Dlk1	Protein delta homolog 1, involved in neuroendocrine and adipocyte differentiation
Esr1	Estrogen receptor, involved in the regulation of eukaryotic gene expression
Gli1	Zinc finger protein GLI1, craniofacial and central nervous system development
Hrk	Activator of apoptosis harakiri, promotes apoptosis
Krt77	Keratin, type II cytoskeletal 1b, unknown
Lypd1	Ly6/PLAUR domain-containing protein 1, a modulator of nicotinic acetylcholine receptors (nAChRs) activity
Magel2	MAGE-like protein 2, regulates the circadian clock by repressing the transcriptional activator activity of the CLOCK-BMAL1 heterodimer.
Myo1h	Unconventional myosin-Ih, intracellular movements.
Nnat	Neuronatin, segment identity in the hindbrain and pituitary development
Nos1	Nitric oxide synthase 1, produces nitric oxide (NO)
Ntsr1	Neurotensin receptor type 1, the activation of downstream MAP kinases
Rprm	Protein reprimo, regulation of p53-dependent G2 arrest of the cell cycle
Scml4	Sex comb on midleg-like protein 4, required to maintain the transcriptionally repressive state of homeotic genes throughout development
Smpdl3b	Acid sphingomyelinase-like phosphodiesterase 3b, strongly influences macrophage lipid composition and membrane fluidity
Trhr	Thyrotropin-releasing hormone receptor, triggers activation of the phosphatidylinositol (IP3)-calcium-protein kinase C (PKC) pathway
Vegfd	Vascular endothelial growth factor D, growth factor active in angiogenesis, lymphangiogenesis and endothelial cell growth
Wdr6	NA (34-2'-O)-methyltransferase regulator WDR6, methylates the 2'-O-ribose of nucleotides at position 34 of the tRNA anticodon loop

e

Down-regulated genes

Gene	Protein and function
Arc	Activity-regulated cytoskeleton-associated protein, a key regulator of synaptic plasticity
Cort	Cortistatin, unknown
Dio2	Type II iodothyronine deiodinase, thyroid hormones metabolism
Dusp4	Dual specificity protein phosphatase 4, mitogenic signal transduction
Dusp6	Dual specificity protein phosphatase 6, dephosphorylation and inactivation of MAP kinases
Egr2	E3 SUMO-protein ligase EGR2, hindbrain segmentation
Egr3	Early growth response protein 3, transcription factor involved in muscle spindle development
Egr4	Early growth response protein 4, transcriptional regulator for mitogenesis and differentiation
Fos	Protein c-Fos, skeletion developemnt of cells
Gpr3	G-protein coupled receptor 3, amyloid-beta peptide generation in neurons
Inhba	Inhibin beta A chain, embryonic development
Npas4	Neuronal PAS domain-containing protein 4, the excitatory-inhibitory balance within neural circuits
Nptx2	Neuronal pentraxin-2, modification of cellular properties that underlie long-term plasticity
Nr4a1	Nuclear receptor subfamily 4 group A member 1, inflammatory response in macrophages
Opn3	Opsin-3, activating G proteins via ultraviolet A (UVA) light-mediated activation
Pdp1	[Pyruvate dehydrogenase [acetyl-transferring]]-phosphatase 1, mitochondrial, unknown
Plekha2	Pleckstrin homology domain-containing family A member 2, unknown
Sdf2l1	Stromal cell-derived factor 2-like protein 1, unknown
Serinc2	Serine incorporator 2, lipid transporter for phosphatidylserine, phosphatidylcholine, and phosphatidylethanolamine
Slc52a3	Solute carrier family 52, riboflavin transporter, member 3, mediating the uptake by cells of the water soluble vitamin B2
Tnfrsf12a	Tumor necrosis factor receptor superfamily member 12A, weak inducer of apoptosis
Tnnc1	Troponin C, slow skeletal and cardiac muscles
Trib1	Tribbles homolog 1, adapter protein involved in protein degradation
Vgf	Neurosecretory protein VGF, neurogenesis and neuroplasticity associated with learning, memory, depression and chronic pain

Extended Data Fig. 7 | Transcriptomic analysis of cerebral cortex from *TAM-N1467D* mice.

a, Experimental design for multi-omics analyses of *TAM-N1467D* mice.

b, Boxplots showing the distribution of log-transformed CPM values across samples before and after filtering.

c, Expression changes of *Scn2a*, immediate early genes and *Esr1*.

d, e Summary of up-regulated (**d**) and down-regulated genes (**e**) in TAM-N1467D mice.

Immediate early genes in bold (**e**).

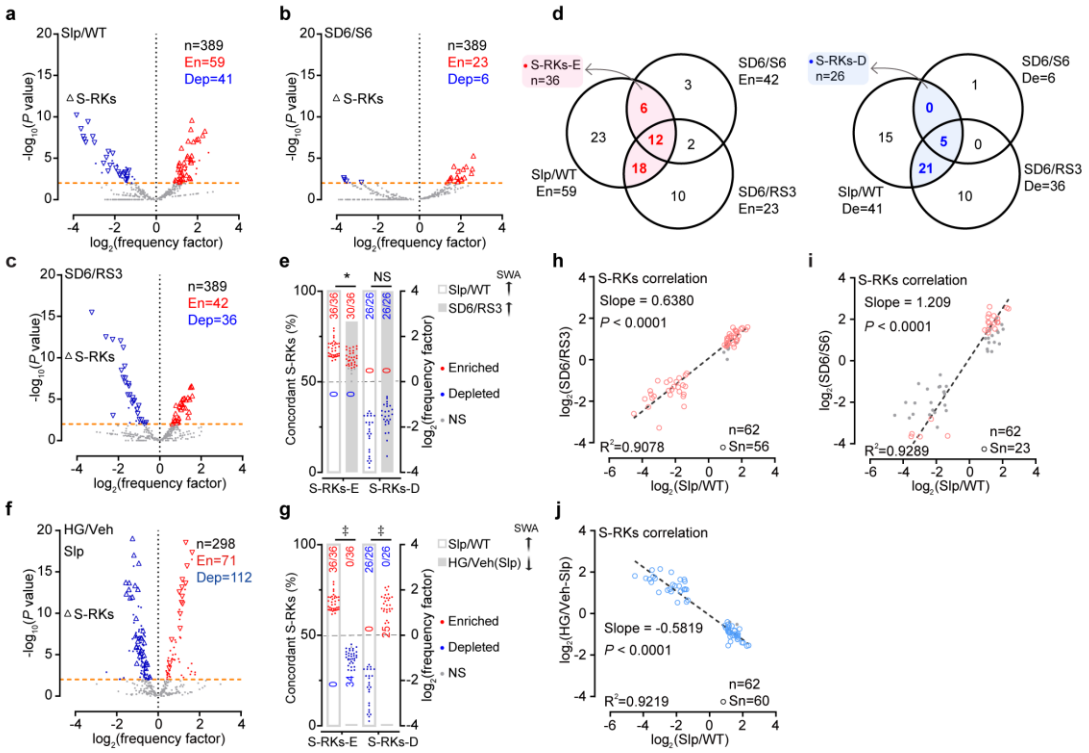

Extended Data Fig. 8 | Analysis approach for kinase motif enrichment in sleep-related signaling pathways.

a-j, Kinase motif enrichment analyses.

Global kinase motif enrichment analysis of Slp/WT(**a**), SD6/S6(**b**), SD6/RS3(**c**) and HG/Veh (Slp) (**f**) comparisons.

Overlapping analysis of Slp/WT(**a**), SD6/S6(**b**), SD6/RS3(**c**) comparisons to identify sleep-related enriched (S-RKs-E, left) and depleted (S-RKs-D, right) kinases (**d**).

Percentage and frequency factor of S-RKs-E (n=36) and S-RKs-D (n=26) for Slp/WT vs. SD6/RS3 (**e**), and Slp/WT vs. HG/Veh (Slp) (**g**) comparison. The fraction of concordant S-RKs was marked at the top of each column.

Correlation analysis of S-RKs significantly enriched or depleted in both Slp/WT and SD6/RS3 (**h**), Slp/WT and SD6/S6 (**i**), Slp/WT vs. HG/Veh (Slp) (**j**) comparisons.

En, enriched; Dep, depleted. Fisher's exact test was used for percentages analysis (**e, g**).

Note: If two comparisons exhibit the same (or opposite) trend in NREMS-SWA, accompanied by a large fraction of concordant (or discordant) S-RKs and a positive (or negative) correlation in S-RKs frequency factor, this indicate that these concordant (or discordant) S-RSs are potential functional signaling pathways in both comparisons.

When using a classic "increased sleep need" model Slp/WT (**a**) as the control comparison, the following observations support the role of S-RKs as potential functional signaling pathways in the respective comparisons: (1) For two other "increased sleep need" model—SD6/S6(**b**) and SD6/RS3(**c**)—S-RKs showed a largely concordant pattern (**e**) and a positive correlation (**h, i**); (2) For the "decreased sleep need" model HG/Veh (Slp) (**f**), S-RKs exhibited a largely discordant pattern (**g**), and a negative correlation (**j**).

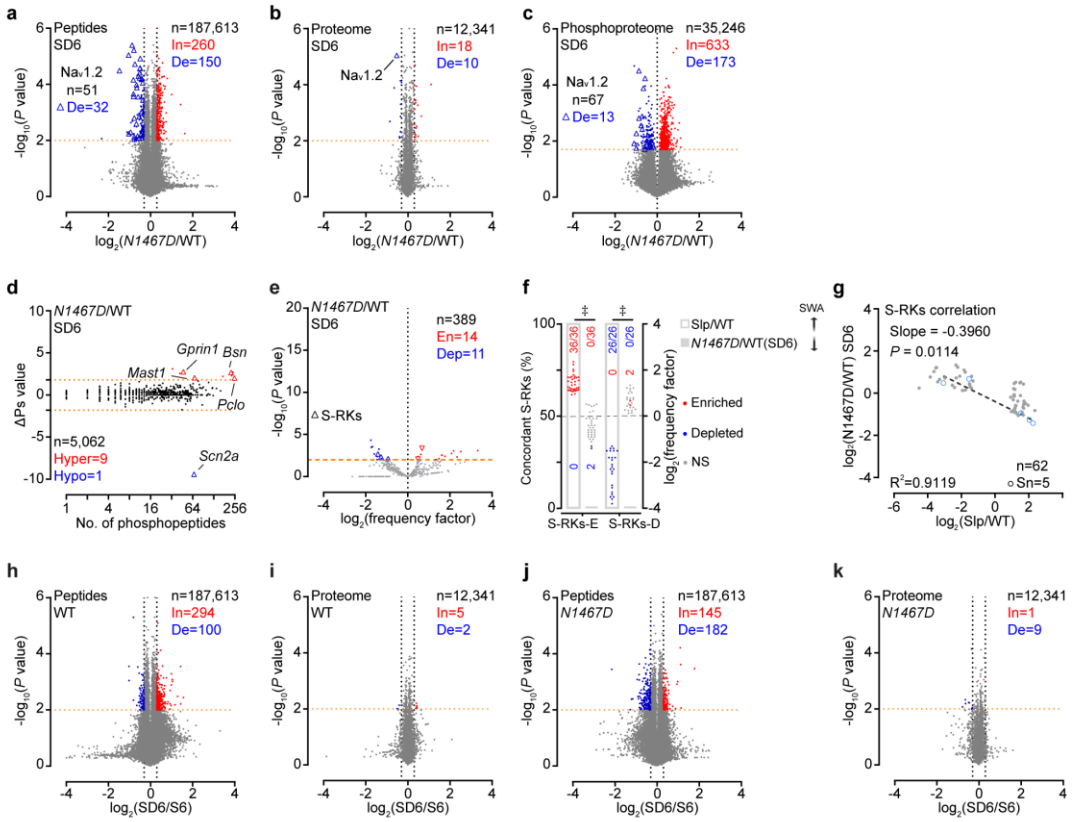

Extended Data Fig. 9 | Proteomic and phosphoproteomic analysis of cerebral cortex from *TAM-N1467D* mice.

a, b Volcano plots illustrating changes in peptide abundance (**a**) and protein abundance (**b**) in the N1467D/WT (SD6) comparison.

c-g, Phosphoproteomic analysis of the *N1467D*/WT (SD6) comparison in phosphopeptide changes (**c**), global ΔPs of phosphoproteins (**d**), global kinase motif enrichment (**e**), percentage and frequency factor of S-RKs (**f**), and correlation analysis of S-RKs (**g**).

h-k, Volcano plots showing changes in peptide abundance (**h, j**) and protein abundance (**i, k**) in SD6/S6 (WT) and SD6/S6 (N1467D) comparisons.

In, increase; De, decrease. Hyper, hyperphosphorylated; Hypo, hypophosphorylated. En, enriched; Dep, depleted.

Multiple unpaired t-test (*P* value) (**a-c**, **h-k**).

Dashed line represents ΔPs = ±1.8 (**d**).

1221 Fisher's exact test was used for percentages analysis (**f**).

1222

1223

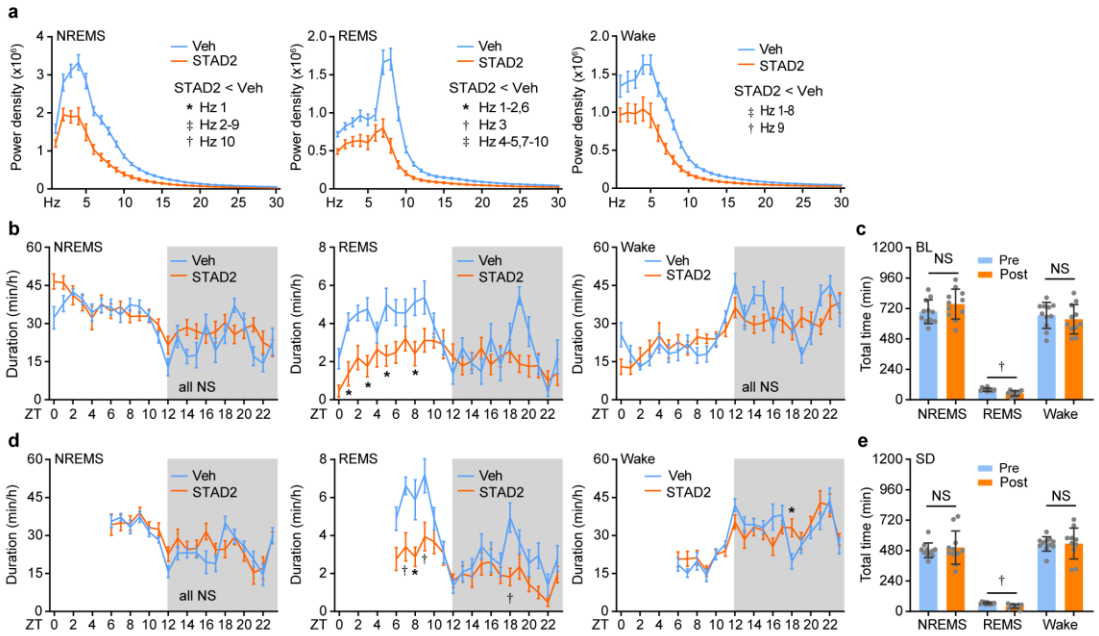

Extended Data Fig. 10 | Sleep analysis of WT mice injected with STAD2.

a-e, Sleep analyses for WT mice (n=11) injected with Veh or STAD2. EEG power spectra (**a**), hourly (**b**) and total time (**c**) for NREMS, REMS and Wake. Hourly (**d**) and total time (**e**) for NREMS, REMS and Wake after 6 h sleep deprivation.

Data shown as mean ± s.e.m. Two-way ANOVA with Sidak's test (**a-b**, **d**) and two-tailed paired t-test (**c**, **e**). * $P < 0.05$; † $P < 0.01$; ‡ $P < 0.001$; NS, not significant, $P > 0.05$.

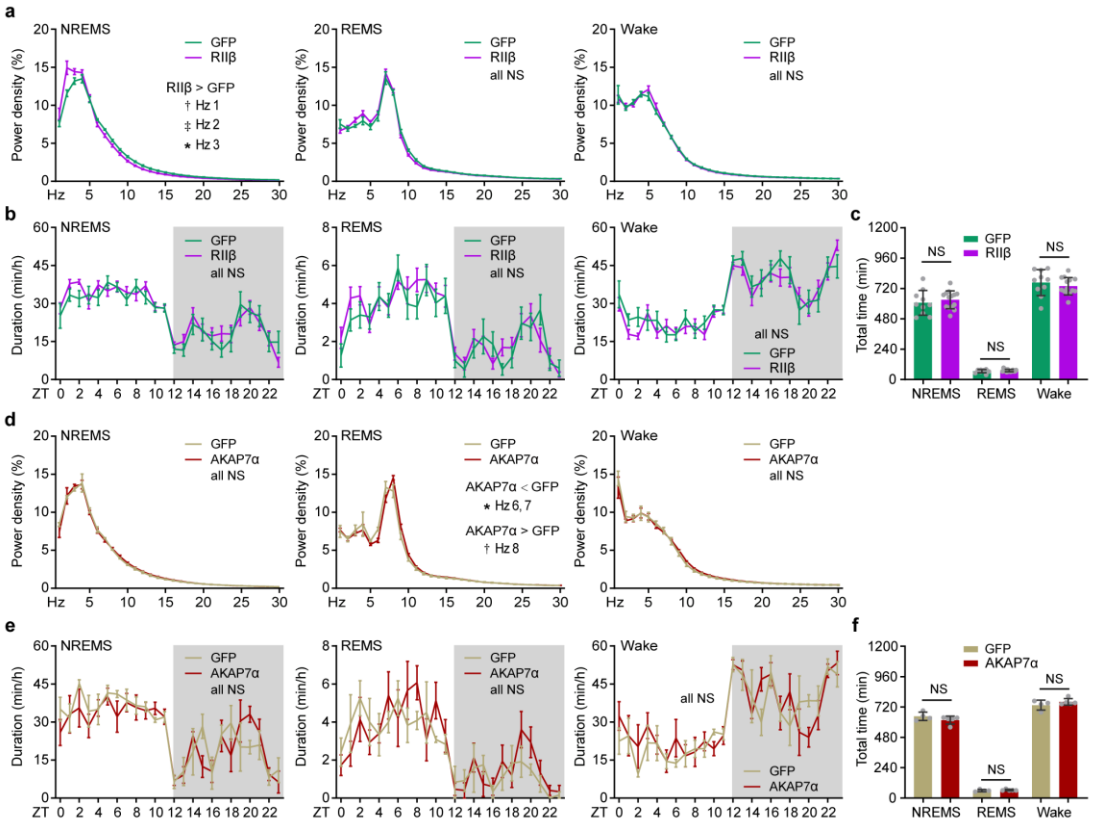

Extended Data Fig. 11 | Sleep analysis of WT mice expressed with RIIβ or AKAP7α.

a-c, Sleep analyses for WT mice expressed with RIIβ. Relative EEG power spectra (**a**), hourly (**b**) and total time (**c**) for NREMS, REMS and Wake. GFP(n=10) vs. RIIβ (n=14). **d-f**, Sleep analyses for WT mice expressed with AKAP7α. Relative EEG power spectra (**d**), hourly (**e**) and total time (**f**) for NREMS, REMS and Wake. GFP(n=4) vs. AKAP7α (n=5). Data shown as mean ± s.e.m. Two-way ANOVA with Sidak's test (**a**-**b**, **d**-**e**) and two-tailed unpaired t-test (**c**, **f**). * $P < 0.05$; † $P < 0.01$; ‡ $P < 0.001$; NS, not significant, $P > 0.05$.

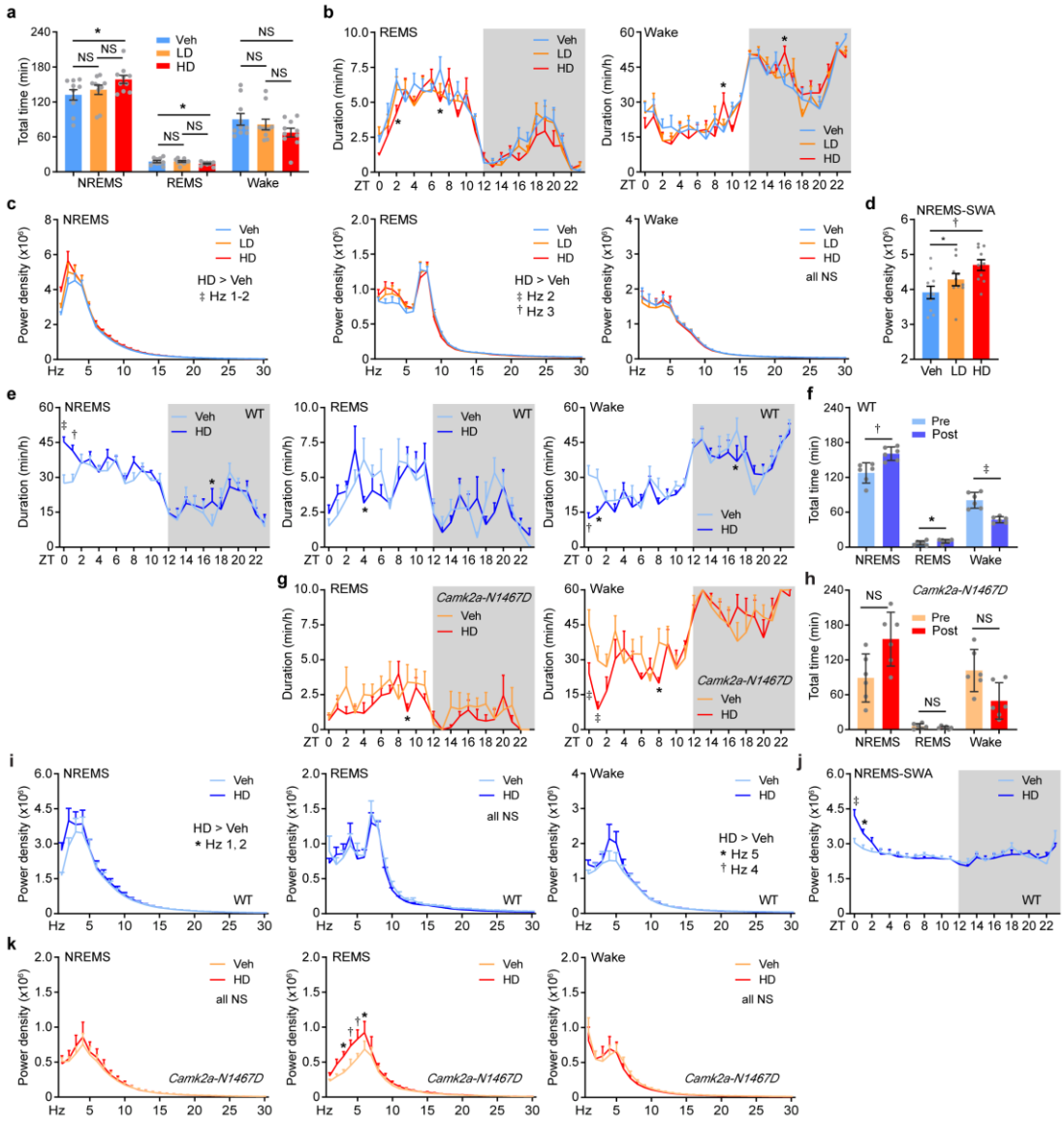

Extended Data Fig. 12 | Sleep analysis of WT mice injected with gabapentin.

a-d, Sleep analyses for WT mice (n=10) injected with Veh or Gabapentin. Total (**a**) and hourly time (**b**), EEG power spectra (**c**) for NREMS, REMS and Wake; quantitative analyses of baseline NREMS-SWA (**d**).

e-h, Circadian (**e, j**) and quantitative (**f, h**) analyses of baseline NREMS in WT (n=6) and *Camk2a-N1467D* (n=6) mice injected with Veh and HD-GBP.

i-k, EEG power spectra (**i, k**) and baseline NREMS-SWA (**j**) in WT (n=6) and *Camk2a-N1467D* (n=6) mice injected with Veh and HD-GBP.

Data shown as mean ± s.e.m. RM one-way ANOVA with Fisher's LSD (**a, d**); two-way

ANOVA with Dunnett's test (**b-c**); two-way ANOVA with Fisher's LSD (**e, g**); two-way ANOVA with Sidak's test (**i-k**) and two-tailed paired t-test (**f**, **h**). * $P < 0.05$; † $P < 0.01$; ‡ $P < 0.001$; NS, not significant, $P > 0.05$.

Supplementary Tables

Supplementary Table 1. List of data for STDPs analysis.

Supplementary Table 2. List of data for RNA-seq and differential expression analysis.

Supplementary Table 3. List of data for quantitative proteomics.

Supplementary Table 4. List of data for quantitative phosphoproteomics. Data list for deltaPs analysis.

Supplementary Table 5. Datasheet for kinase motif-enrichment analysis.

Supplementary Table 6. Data list for prediction of PKA site in Nav1.2.

Supplementary Table 7. Statistical Analysis. Complete sample sizes, statistical test methods, and precise result values are reported for all comparisons.